Version 1.8
ELECTROWEAK/ANAL/CDFR 1349
April 5, 1991

W/Z Cross Sections in the Muon Channel

S. Eno, D. Kardelis, D. A. Smith, R. Swartz

Abstract

An analysis of high transverse momentum muons yields the ratio of the W and Z production cross sections times branching ratios, $R = \sigma(W \to \mu\nu)/\sigma(Z^\circ \to \mu^+\mu^-) = 9.6 \pm 1.1(stat) \pm 0.5$ (sys), where the statistics of the Z sample dominates the uncertainty. We find the cross section $\sigma(W \to \mu\nu) = 2.29 \pm 0.07(stat) \pm 0.12(sys) \pm 0.15(lum)$ nb, with the dominant uncertainty coming from the luminosity measurement, and $\sigma(Z^\circ \to \mu^+\mu^-) = 0.238 \pm 0.023(stat) \pm 0.009(sys) \pm 0.016(lum)$ nb. Details of the muon identification, acceptance, efficiency, and backgrounds are presented. The results are shown to be in good agreement with the predictions of the standard model.

Contents

List of Tables

List of Figures

1 Introduction

In the standard model, W and Z bosons are produced in $p\bar{p}$ collisions via the lowest-order Drell-Yan process, $q\bar{q} \rightarrow W(Z)$, and by radiative QCD processes producing a quark or a gluon in the final state. A measurement of the production rate therefore tests the quark-boson couplings, the parton momentum distributions, and higher-order corrections. Subsequent leptonic decay of the W and Z depends on the lepton-boson couplings, the boson masses, the Top quark mass (for $M_{top} < M_W$) and the existence of additional fermion generations. Comparison of predicted rates with measured rates thus tests many aspects of QCD and the standard model.

For N candidate events and B background events, the absolute cross-section,

$$\sigma = \frac{N - B}{\epsilon A \int \mathcal{L} dt} \tag{1}$$

is subject to large systematic uncertainties in the integrated luminosity, $\int \mathcal{L} dt$, the detection efficiency ϵ and the acceptance A. To first order, most of these uncertainties cancel in the the cross-section ratio,

$$R = \frac{\sigma(W \rightarrow \mu\nu)}{\sigma(Z^\circ \rightarrow \mu^+\mu^-)} = \frac{\sigma(p\bar{p} \rightarrow WX)}{\sigma(p\bar{p} \rightarrow Z^\circ X)} \frac{\Gamma(W \rightarrow \mu\nu)}{\Gamma(Z^\circ \rightarrow \mu^+\mu^-)} \frac{\Gamma(Z^\circ)}{\Gamma(W)} \tag{2}$$

especially if the same muon identification cuts are used for the muon from the W and one of the muons from the Z. We focus on the R measurement to obtain greater sensitivity to the underlying physics.

Previously, CDF has measured the W and Z cross sections and R in the electron channel [1,2,3,4]. This note describes the muon analysis. Extending the previous work to include muons gives a smaller statistical uncertainty, from the increased statistical power of the combined $Z^\circ \rightarrow ll$ sample, and a smaller systematic uncertainty since the lepton identification and some of the backgrounds are different for the two analyses. Furthermore, for large M_{top} the Top quark decays into real W particles so that detailed understanding of W events is prerequisite to quantitative Top measurements.

A and ϵ in equation (1) are the products of several factors, coming from geometric and kinematic cuts as well as from trigger and chamber performance and from cuts made in the offline analysis. A more specific relation for the $W^\pm$ cross-section is

$$\sigma(W \rightarrow \mu\nu) = \frac{N_W}{\int \mathcal{L} dt} = \frac{1}{\int \mathcal{L} dt} \frac{(N_W^{obs} - B_W)}{A_W \cdot T \cdot \epsilon_g \cdot \epsilon_{cos}} \tag{3}$$

where A_W combines the kinematic and geometric acceptance for W events, T is the trigger efficiency, ϵ_{cos} is the efficiency of the cosmic ray filter for W and Z events, and ϵ_g is the combined efficiency of the cuts defining a 'gold' muon. A 'gold' muon passes the tight selection criteria that are applied equally to the W muon and to one of the muons from the

Z decay. The second Z muon passes looser cuts, and this 'silver' muon has a higher efficiency ε_s.

The Z cross-section calculation is more complicated because for events where both tracks pass through the muon chambers, either can satisfy the trigger and gold identification requirements, whereas for events where one track misses the muon chambers only one muon can. The terms are

$$A_{00} \cdot \varepsilon_{CMUO} \cdot T(2-T) \cdot \varepsilon_g(2\varepsilon_s - \varepsilon_g) \cdot \varepsilon_{cos} \tag{4}$$

$$A_{00} \cdot 2(1-\varepsilon_{CMUO}) \cdot T \cdot \varepsilon_g \varepsilon_s \cdot \varepsilon_{cos} \tag{5}$$

$$A_{0X} \cdot T \cdot \varepsilon_g \varepsilon_s \cdot \varepsilon_{cos} \tag{6}$$

The first term counts events where both tracks project to the muon chambers and have a stub in the muon chambers. The second counts events where both tracks project to the muon chambers, but only one has a stub. The third counts events where one track projects to the muon chambers and has a stub there, but the other projects beyond the end of the muon chambers or into a crack. ε_{CMUO} is a small correction to allow for stub pattern recognition inefficiencies in the muon code and for tracks predicted to hit the muon chambers in the Monte Carlo but that multiple scatter out in the data. The middle term makes a very small contribution, the relative magnitudes of the three terms being 41 : 1 : 81.

The advantage of the R measurement is apparent when we form the ratio of the W and Z relations, and several factors cancel. The result is

$$R_\mu = \frac{(N_W - B_W) \cdot [A_{00}\varepsilon_{CMUO}(2-T)(2\varepsilon_s - \varepsilon_g) + 2A_{00}(1-\varepsilon_{CMUO})\varepsilon_s + A_{0X}\varepsilon_s]}{(N_Z - B_Z) \cdot A_W} \tag{7}$$

With these equations, the cross-section measurement reduces to the task of determining all the various contributions to the above N's, A's, B's, and ε's. The rest of this note describes how we determined these values, summarized in table 8.

2 Data Sample

The data sample used for this analysis has been described in detail in [5,6,7]. Here, we review the main points.

Beginning with the 5.1 Production muon output (MUO04, see [5]), we require at least 1 CMUO with non-beam-constrained $p_t > 18$ GeV/c, track-to-stub matching $|dx| < 10$ cm, consistent with a minimum ionizing particle (deposition in the hadron tower traversed by the muon < 6 GeV, and < 2 GeV in the electromagnetic calorimeter tower). A CMUO is a stub in the central muon chambers matched to a CTC track. A stub must have hits in 2 of the 4 chamber layers, if there are more than 2 hits then 3 must be collinear within 2 mm in the $r\phi$-direction. Reference [8] provides a road map to the muon pattern recognition code. The CTC track is required to pass quality cuts, namely, it passes TRKSEL, has impact

parameter < 1 cm, and goes through super-layer 5 or attaches to a VTPC track. This leaves 11485 events.

We retrack with PUBLIC tracking, beam-constrain with CTCSBM, and re-run CENMUO [8] using the beam-constrained parameters to re-calculate track-stub matching, energy deposition, etc. The new parameters are stored in the CMUO/CMIO banks. (A CMIO is any track with $p_t > 10$ GeV which passes the track quality cuts mentioned above and is not a CMUO. These extend the Z acceptance beyond the ends of the muon chambers and into the phi, etc. cracks.)

Beginning with the above sample, the 'standard' data sets

CDF$W_Z_DATA:[ANA]CENTRAL_MUO_I.EVT,
CDF$W_Z_DATA:[ANA]CENTRAL_MUO_II.EVT

come from applying the following cuts (some of which have been applied before the CMUO banks were remade. If events were lost from this double-tracking procedure, this would be accounted for by ϵ_{CMUO}. However, we have seen no evidence that this occurs.) The cuts are:

1.) reject runs with the broken muon trigger (NRUN< 17265 and NRUN= 17278, see [26]), and C$ELE:BADRUNs, that have funny $\not\!\!E_T$ distributions [11];

2.) Event is not a cosmic ray event, defined as an event which contains an isolated high-Pt CMUO/CMIO which fails the cosmic ray filter (see [15]);

3.) Event contains a CMUO which

   a) has track-to-stub matching $|dx| < 10$ cm;

   b) has $E^{EM} < 2$ GeV and $E^{had} < 6$ GeV in the muon tower;

   c) has non-constrained $p_t > 18$ GeV/c;

   d) is beam-constrainable with CTCSBM, and has constrained $p_t > 20$ GeV;

   e) has $|z_0 - z_{vtx}| < 5$ cm for some $p\bar{p}$ vertex with $|z_{vtx}| < 60$ cm;

   f) is in the fiducial region (FIDCMU=0).

FIDCMU is a routine that extrapolates CTC tracks to the radius of the muon chambers, and tells whether the track traverses the chambers, cracks, endwall, or misses the muon fiducial region, see [10]). This leaves 3425 events, including non-isolated muons used in the background studies. A 'golden' muon passes all of the above and, in addition,

- $|dx| < 2$ cm
- $ISO < 0.1$ where

$$ISO = \frac{\sum_{0.4} E_t - E_t^{\mu}}{p_t^{\mu}} \tag{8}$$

and $\sum_{0.4} E_t$ is the transverse energy in a cone of $\Delta R < 0.4$ around the muon (see appendix A), E_t^μ is the transverse energy deposited in the tower traversed by the muon (see appendix B), and p_t^μ is the beam-constrained transverse momentum of the muon track. [1]

- muon stub not in wedge 17E for runs 20278-20446 (HV problem, see [26]).
- muon stub not in the middle chamber of wedge 2E, where we observed bad stub measurements in the drift direction.

Figure 1 shows distributions of the main variables used to define the W sample. Figure (a) shows the energy deposition in the calorimeter tower traversed by the muon for W events(no trigger requirement). Figures (b,c,d) show the dx, ISO, and MET distributions when all other cuts are applied except the one in the variable plotted (no trigger requirement). Figure 2 shows distributions of the main variables used to define the W sample. Figure (a) shows the energy deposition in the calorimeter tower traversed by the muon for Z events. Figures (b,c) show the dx, ISO when all other cuts are applied except the one in the variable plotted. Small corrections to the acceptance compensate for the 17E (about 0.1%) and 2E problems (about 0.7%). Figure 3 illustrates the 2E problem, showing that the matching distribution for this wedge is unusually wide, and that almost all the muon candidates failing the matching cut for that wedge come from the middle chamber of the three chambers.

A Z-candidate event has 1 golden muon, and another CMUO or CMIO which passes cuts 3b-3e, above, and passes completely through SL8 of the CTC (FIDCMU$\neq$ 6). There are 117 such events, with the invariant mass distribution shown in figure 5. 109 events are in the window $65 \leq M_{\mu\mu} \leq 115$ GeV/c^2. 1 event failed the central muon trigger, leaving 108 Z-candidates.

A W-candidate has 1 golden muon, $\not\!\!E_{\rm T} > 20$ GeV and is not in the Z sample. $\not\!\!E_{\rm T}$ is corrected for the golden muon according to

$$\not\!\!E_{\rm T} = \sqrt{\not\!\!E_{{\rm T}_x}^2 + \not\!\!E_{{\rm T}_y}^2}, \qquad \text{where} \tag{9}$$

$$\not\!\!E_{{\rm T}_x} = METS_x - p_x^\mu + E_t^\mu \cos\phi_\mu \tag{10}$$

$$\not\!\!E_{{\rm T}_y} = METS_y - p_y^\mu + E_t^\mu \sin\phi_\mu. \tag{11}$$

$METS$ is the calorimeter missing E_t from the METS bank. This gives 1438 events with the transverse mass distribution shown in figure 4. 6 of these are Z events where the second muon failed the minimum ionizing cut, but have $ISO < 0.2$. 1 event did not satisfy the central muon trigger, leaving 1431 W-candidates. Figures 4 and 5 show the transverse mass and invariant mass distributions of our final W and Z samples, respectively. Figures 6

[1] The variable ISO was chosen for this analysis for historic reasons, mainly in an attempt to be consistent with the electron analysis and thereby to save time. The authors recommend AGAINST the use of ISO in future W, Z analyses. Rather, we recommend using the border tower energy $BTE = (\sum_{0.4} E_t - E_t^\mu)$ instead. See [17] for precedent.

and 7 show the transverse momentum distributions of the muons in the W and Z samples, respectively.

3 Acceptances

Detector geometry and kinematic cuts on the boson decay products limit the observed number of bosons. Monte Carlo methods are used to calculate the acceptance, which divide naturally into 4 terms:

A_W: $W^{\pm}$ candidate events are selected by requiring $p_t^{\mu} > 20$ GeV/c and $\not\!\!E_T > 20$ GeV. The muon chambers cover roughly $|\eta| < 0.6$.

A_{00}: Z events where both tracks traverse the muon chambers have higher detection and selection efficiencies.

A_{0X}: Z events where only one track hits the muon chambers are detected by looking for a high p_t track traversing all 9 CTC superlayers, with a calorimeter signal consistent with a minimum ionizing track. The second muon is in a different rapidity region or a ϕ crack, so these events must be treated separately from the A_{00} events.

A_{ZW}: Z events where one muon is golden, the second track is beyond the Z η acceptance, and the event passes the W $\not\!\!E_T$ cut (for W background calculations).

3.1 Monte Carlo and Detector Simulation

Campagnari's montecarlo [18] generates W or Z events using zero-order diagrams to produce bosons over a range of 10 mass widths. This 'toy' monte carlo is fast, permitting high-statistics studies of the effects of varying parameters. The main steps in the monte carlo are:

1. Zero-order diagrams produce bosons with no transverse momentum. For Z's we boost the decay products using p_t of the boson taken randomly from J. Ng's $d\sigma/dp_t$ distribution [22]. For W's we use Winer's $W \rightarrow e\nu$ $d\sigma/dp_t$ distribution [21]. The spectra are acceptance and resolution corrected and have the same shape within errors;
2. Smear the decay vertex with $\sigma = 30.0$ cm, require $|z_{vtx}| < 60.0$cm;
3. Smear the curvature with $\sigma = 0.0021$;

For the Z's, we then randomly select the charge of the first decay muon, assign the opposite charge to the other, and apply the 20 GeV/c p_t cut to both. FIDCMU [10] calculates where the track went, i.e., chambers, phi cracks, beyond the chambers, etc., and we tally the numbers of events with legs in the various acceptance zones. The simulation does not include multiple scattering. Note that we include the number of Z events where one

muon hits the chambers but the other is beyond our η cut, to calculate the W background due to these 'one-legged' Z's (the A_{ZW} term). These 'one-legged' Z's make it into the W sample, because the $\not\!\!E_T$ is only corrected for the p_t of the 1 muon which is seen.

As a check, we compare the ratio A_{0X}/A_{00} from the Monte Carlo with the observed number of events N_{0X}/N_{00} in the data, corrected for efficiency. Recall that the 00 subscript means that both muons traverse the chamber fiducial region, while $0X$ means that the second track goes into a crack or beyond the end of the chambers (but still traverses all CTC superlayers). The result is summarized in figure 8, where η is calculated for the point where the track leaves the CTC volume. The two curves agree well until around $\eta \sim 1.0$ or 1.1, where CTC efficiency begins to suffer as tracks leave the CTC without hitting all axial superlayers. This agrees with previous work (see [12,13,14]) as well as figure 9.

For W's, we make the 20 GeV/c p_t cut on the decay muon. The 20 GeV/c $\not\!\!E_T$ cut requires more attention. We smear $\not\!\!E_T$ using the model developed for the W mass measurement and described in detail in reference [20] before applying the $\not\!\!E_T$ cut. The model reproduces the effects of both the underlying event and the detector response. The mass analysis uses a no-jet cut whereas the present analysis keeps jets. Hence we replaced the $\sum E_t$ distribution used as monte carlo input with one taken from our data sample. We then find good agreement between underlying event parameters for the data and from the monte carlo, as shown in figure 10. The underlying event E_t is the vector sum of all E_t in the event, after removing the W. Figure 10 shows the magnitude, the component parallel to the muon direction, and the component perpendicular to the muon direction, for both the W data (dashed histogram) and the monte carlo (solid), normalized to the number of W events. Handling the $\not\!\!E_T$ smearing this way means that the efficiency of the $\not\!\!E_T$ cut is included in A_W, as distinct from the electron analysis where the effect was kept separate.

Acceptance is first calculated using optimum parameters. That is, we run the zeroth order monte carlo with the nominal fiducial coverage, $\sum E_t$, boson p_t, and so forth. This yields the results listed in table 1. We then study the effects of varying the various inputs, as described in the next section. Table 8 lists the final values after applying the corrections and combining the errors.

3.2 Systematic Studies

The acceptance error comes from uncertainties in the Monte Carlo inputs. They are

- contributions from higher-order diagrams,
- the structure functions,
- our modeling of the underlying event for W's,
- the boson p_t spectrum, and
- $sin^2\theta_W$.

- tracking resolution

The toy monte carlo uses lowest-order diagrams only, and must be corrected for the contributions from the higher-order graphs. The higher order terms change the p_t and rapidity distributions of the decay products and thus the acceptance. The first order corrections to the total cross section are quite large being approximately 30% at the Cern energy of 630 GeV and decreasing at higher energies. At $\sqrt{1.8}$ TeV, the correction is about 20%, depending weakly on the mass factorization scheme used. In the different schemes the various graphs contribute in different proportions, although the results agree within about 5%. Being such a large correction, theorists have checked the second order corrections and find it is comparable to the uncertainty due to structure functions. In at least one factorization scheme, the second order correction reduces the dependence of the results on the choice of the factorization scale [19].

To account for the higher order contribution we turn to PAPAGENO. The Papageno monte carlo generates $W + n$-jet events to $\mathcal{O}(\alpha^3)$ for $n = 0, 1$. We first run the zero-jets case and confirm the results from the toy monte carlo. Zeroth order Papageno gives 18.21 $\pm$ 0.13, while the toy MC gives 18.17 $\pm$ 0.12. (With the 17E correction listed below, this becomes 18.15, as in table 3.) We then generate $W + 1$-jet events, calculate the acceptances as before, and weight the Papageno and toy Monte Carlo results in the proportion 20:80 to obtain the values listed in table 3. We assign the resulting uncertainty the same magnitude as the correction.

Note that approximately 30% of the events in data have a jet with $E_t > 10$ GeV, and one might argue that this is the correct proportion of higher-order acceptance to include. However, the effect of the correction is small enough that using 20% or 30% does not affect our conclusions.

Repeating the acceptance calculation for 5 different structure functions gives the variation listed in table 2. None of the structure functions disagrees significantly with the others for all of the acceptance terms, and we use the weighted average of the different results.

Acceptance term	Toy M.C.	Papageno 1 jet	Combined
W acceptance (A_W)	$18.15 \pm 0.12\%$	$18.09 \pm 0.13\%$	$18.14 \pm 0.12\%$
Z acceptance			
Fiducial/Fiducial (A_{00})	$4.52 \pm 0.07\%$	$4.77 \pm 0.07\%$	$4.57 \pm 0.07\%$
Fiducial/Non-Fiducial (A_{0X})	$10.33 \pm 0.10\%$	$10.79 \pm 0.11\%$	$10.42 \pm 0.10\%$
'One-legged Z's' (A_{ZW})	$20.11 \pm 0.13\%$	$19.48 \pm 0.14\%$	$19.98 \pm 0.13\%$

Table 1: Acceptances, including 17E correction, with statistical errors only.

The boson polarization, and hence the angular distribution of the daughters, depends on $sin^2\theta_W$. The value measured at LEP contains the effects of the higher-order

Structure function	A_W	A_{00}	A_{0X}	A_{ZW}
MRSE	18.28 ± 0.12	4.53 ± 0.07	10.43 ± 0.10	20.10 ± 0.13
MRSB	18.61 ± 0.12	4.64 ± 0.07	10.35 ± 0.10	20.56 ± 0.13
DO1	17.85 ± 0.12	4.45 ± 0.07	10.33 ± 0.10	19.99 ± 0.13
DO2	17.49 ± 0.12	4.47 ± 0.07	10.17 ± 0.10	20.15 ± 0.13
EHLQ	18.67 ± 0.13	4.57 ± 0.07	10.36 ± 0.10	19.90 ± 0.13

Table 2: Structure function dependence of W acceptance.

radiative processes, and hence is appropriate for our use (instead of deriving a value from our M_W measurement). The value of the weak mixing angle is $sin^2\theta_W = 0.2272 \pm 0.0040$. To evaluate the effect on the Z acceptance terms, we re-calculated replacing the nominal $sin^2\theta_W$ value in the Z Monte Carlo with the 1σ extrema. For the W acceptance we varied M_W within the errors bars. (The Z Monte Carlo makes no explicit reference to M_W and the W Monte Carlo does not include θ_W.) The results are in table 3.

We varied the momentum scale of the boson p_t spectrum by 20% to find the acceptance uncertainty listed in the table. Figure 11 shows the boson p_t dependence of the Z acceptance terms. As p_t^Z increases the lab angle between the daughter muons shrinks, and when the angle is a multiple of 15° (one wedge) then A_{00} hits a local minimum and A_{0X} is a maximum.

We repeated the acceptance calculations varying the parameters in the underlying event model. There are three main parameters in the model. First, the measured p_t of the W is degraded by a factor of 1.4 relative to the true W p_t to account for the calorimeter non-linearities and for magnetic sweeping. Then, this degraded p_t is smeared with $\sigma = 0.83$ to take into account the energy resolution of the calorimeter. Finally, an underlying event vector is added, whose x and y components are randomly chosen from a gaussian distribution with an RMS equal to 0.47 times the square root of the total scalar E_t in the event. We vary the non-linearity parameter, the energy resolution parameter, and the underlying event parameter by 20%. The results are summarized in Table 3.

Wedge 17E was without negative high voltage during two weeks of data taking. We reject boson candidates in that wedge during those runs (a few events), and make a correction to the acceptance. Naively, this correction is one wedge in 48, times the fraction of our luminosity taken during those two weeks, 0.2 pb^{-1} out of 3.54 pb^{-1}, or 0.1%. Z events, with two legs, are slightly more complicated, the actual correction factors are A_W : 0.9989, A_{00} : 0.9978, A_{0X} : 1.000, and A_{ZW} : 0.9985. The values in table 1 have been corrected, those in table 2 have not.

We varied the tracking resolution used in the simulation from $\delta p_t/p_t^2 = 0.0011$ to 0.0021 and found no effect on the acceptance, as is shown in figure 12.

Term	High-order error	Structure functions	ΣE_T Event	Boson p_t	$sin^2\theta_W$ $(* \Rightarrow M_W)$	Under. Event	Total
A_W	0.01	0.6	0.02	0.04	0.2*	0.15	0.7
A_{00}	0.05	0.1	-	0.02	0.1	-	0.2
A_{0X}	0.09	0.1	-	0.07	0.2	-	0.3
A_{ZW}	0.13	0.3	0.03	0.16	0.1	0.28	0.5

Table 3: Acceptance systematics. Units are $100 \times \delta A$.

4 Efficiencies

Seven sources contribute to our boson detection efficiency, and are listed in table 4. The cut on the muon stub/CTC track match, and the cut on the energy deposition in the calorimeter tower, were studied using cosmic ray, J/ψ, and W/Z data as described in references [23,24]. The effect of the cosmic ray filter is briefly described in the 'background' section of this note, and in detail in [15]. This section covers the remaining factors.

Cut Type	Measured Efficiency
matching< 2 cm	$\varepsilon_{dx} = 96.0 \pm 1.0\%$
Min. ioniz. cut	$\varepsilon_{m.i.} = 98.7 \pm 0.2 \pm 0.2\%$
$ISO < 0.1$	$\varepsilon_{iso} = 98 \pm 1\%$
re-tracking	$\varepsilon_{trk} = 98.7 \pm 1.0\ \%$
Stub finding	$\varepsilon_{CMUO} = 98.6\binom{+1.2}{-3.3}\%$
Cosmic filter	$\varepsilon_{cos} = 99.7 \pm 0.2$
Muon Trigger	$T = 91 \pm 2$
Combined "silver"	$\varepsilon_s = \varepsilon_{m.i.}\varepsilon_{trk} = 97.4 \pm 1.0\%$
Combined "gold"	$\varepsilon_g = \varepsilon_s\varepsilon_{iso}\varepsilon_{dx}\varepsilon_{CMUO} = 90.4 \pm 3.4\%$

Table 4: Efficiencies.

4.1 Trigger Efficiency

The central muon trigger efficiencies have been carefully studied and documented by Alain Gauthier [26,27,28,29]. For the present analysis two small corrections need to be considered.

First, the efficiency falls off near the ends of the chambers. This is apparent in figure 13. If muons are required to be a few cm away from the chamber ends, the Level 1 trigger efficiency increases by about 0.5%. The fiducial cuts applied to the W and Z samples

[7,11] restrict the muons to the high-efficiency zone, hence we re-evaluated the L1 trigger efficiency using Gauthier's data set and FIDCMU. The Level 1 efficiency for fiducial muons is $93.4 \pm 0.5\%$. Combining this result with the Level 2 and 3 results gives an overall trigger efficiency of $91.0 \pm 2.0\%$.

Figure 13 shows an efficiency plateau at $\sim 94.1\%$, or 1.8% higher than the value in [27] (dotted line). The difference is that in order to plot the z-position of the muon stubs, events with ADC overflows had to be rejected. ADC overflows can be caused by knock-on electrons produced as the muons pass through the aluminum chamber walls. If the muon bremstrahlungs in the hadron calorimeter, the leakage particles from the photon shower can give multiple hits on a sense wire, causing ADC overflow. If there is a jet at the same phi as the muon, the ADC overflow can be caused by jet leakage. This is not an important effect for muons from W and Z decay, which are isolated, but could be significant for muons from b meson decay. We observe that 4% of the muon-candidates have ADC overflows in the cosmic ray data. The rate in $p\bar{p}$ data depends on the cuts used to identify good muon events, ranging from 1.8% to 7%. This could affect our estimate of the trigger efficiency by a half- to one-percent, which is completely negligible in the final analysis. We therefore assign an additional systematic error of $\pm 0.5\%$ to the trigger efficiency based on the variation in ADC overflow rates. (Note that we do not make any explicit ADC cuts in the W/Z samples.)

Z events with both muons hitting the chambers provide another check of both the Level 1 and Level 2 trigger efficiencies. One muon must be a gold muon with a L2 trigger, the other a CMUO with $E^{EM} < 2$, $E^{had} < 6$, $p_t^{\mu} > 20$ GeV and not be in chamber 2E-B or in wedge 17-E for runs 20278-20446 and have a invariant mass between 65 and 115 GeV/c^2. Of these second muons, 66 out of 70 fired the L1 trigger, or $94.3\left(^{+2.7}_{-4.3}\right)\%$. Requiring the second muon to be in the chamber fiducial region changes the result slightly, $61/64 = 95.3\left(^{+2.5}_{-4.4}\right)\%$. These are consistent albeit slightly higher than Gauthier's result of $92.3 \pm 0.5\%$ from cosmic ray data [27].

Taking the same Z sample and looking at the Level 2 trigger information gives a Level 2 result of $64/66 = 97.0\left(^{+2.0}_{-3.9}\right)\%$ and, if we require the second muon to extrapolate to the chamber fiducial region, $59/61 = 96.7\left(^{+2.1}_{-4.2}\right)\%$, in great agreement with the Level 2 result of $97.2\left(^{+1.5}_{-2.6}\right)\%$ cited in [28]. Requiring further that both the Level 1 and Level 2 triggers fired gives a combined L1*L2 result of $64/70 = 91.4\left(^{+3.4}_{-4.8}\right)\%$, which becomes $59/64 = 92.2\left(^{+3.3}_{-4.9}\right)\%$ for fiducial second muons. This confirms the $91 \pm 2\%$ result nicely.

As another check, we took Gauthier's data sample of high p_t muon events having a trigger independent of the CFT [28], applied the same the same selection cuts used in the Level 2 study while adding the same fiducial requirement used for the W and Z sample, and re-evaluated the trigger efficiency, finding $97.2\left(^{+1.5}_{-2.6}\right)\%$ for the level 1 trigger. This is higher than but consistent with the cosmic ray value above. Using only runs in this sample where the the L2 trigger was working properly, the L1*L2 trigger efficiency is found to be $92.7^{+2.5}_{-3.4}\%$ in agreement with the L1*L2 result given above.

4.2 Tracking Efficiency

CTC track reconstruction code uses two different algorithms optimizing different things. Berge's programs emphasize precision, obtained by finding the sets of hits giving the best fits, and is good for mass measurement. Mukherjee tends to reject kinked tracks, as from decay-in-flight events, which is good for cross-section work. PRODUCTION tracking uses both to obtain highest efficiency. PUBLIC at this time uses Mukherjee's code, and we found that PUBLIC reduces our background appreciably. This is why we re-tracked our data sample. Figure 14 shows an estimate of the QCD background in the W-sample for the two kinds of tracking. Many of the tracks rejected by PUBLIC were identified as decay-candidates in hand-scanning, as suggested by figure 15, which shows characteristics of tracks present in the PRODUCTION sample but lost when we re-tracked with PUBLIC. The offsets in the dx distribution are typical of low p_t tracks assigned a large p_t in reconstruction. The low hit multiplicity of the lost tracks is typical of tracks that were most accurately fit in two halves.

Unfortunately, a database error present at the time we re-tracked gave the wrong beam position, spuriously degrading the tracking resolution in our sample. Figure 16 shows the dimuon mass distributions for a sample of 148 $Z^\circ \rightarrow \mu^+\mu^-$ candidates, using PRODUCTION tracking and using the tracking in our data sample. This error does not affect the conclusions of the cross-section measurement, since we measured the various biases from our sample, and handled the monte carlo consistently.

Re-tracking brings a small cost in efficiency. We studied the efficiency by retracking the official electron Z sample. Out of 237 electrons which had tracks in this sample, 3 were lost, giving $\varepsilon_{trk} = 0.987 \pm 0.01$.

We then verified that the tracking efficiency is flat over our A_0X acceptance region for the original (SPIN) tracking. Previous studies of the η dependence of tracking efficiency can be found in references [12,13,14]. We selected a sample of $Z^\circ \rightarrow e^+e^-$ events with no tracking requirement on the second electron. We then looked to see how often a track passing our cuts points at the calorimeter cluster. Tracks at smaller polar angle exit the CTC without traversing all superlayers and have lower reconstruction efficiency. We define the exit radius pseudorapidity as

$$\eta_e = -\log(tan\frac{\theta}{2}) \quad \text{where} \tan\theta = r_e/z_0.$$

Here, r_e is the radius of the track when it leaves the CTC, and z_0 is the distance along the beam from the center to Z position of the track when it leaves the CTC. The η_e range for the second Z muon is chosen so that the efficiency is flat.

In detail, we started with CENTRAL_ELEC_I and CENTRAL_ELEC_II [9], bad runs were rejected [11], and events with 1 fiducial (including BADTOW) electron passing the electron R analysis golden electron criteria were kept. This includes a 20 GeV cut on the electron p_t. In addition to the normal "golden" electron identification cuts, we required the electron track (1^{st} leg) to come from the main event vertex and have $\sum p_t/p_t < 0.1$ for

a cone of $\Delta R = 0.4$ around the electron(track isolation). We call electrons which pass the "golden" cuts plus these additional cuts "platinum" electrons. We then looked for another ELES cluster in the event with $E_t > 18$ GeV, HAD/EM < 0.07, and ISO< 0.1. If there is more than 1 such cluster, we pick the cluster which, when paired with the first electron, makes a mass closest to the Z mass. We require $86 < M_{ee} < 96$ GeV/c^2. Fiducial cuts are not made on the second electron because FIDELE requires a track associated with the cluster for central electrons.

Then, for each platinum electron, the other electron goes into the efficiency calculation. An electron is considered to have a track associated with it if:

1.) pointer TRPELE does point to a track, and the track passes TRKSEL;

2.) E/P< 2

3.) $\delta\phi < 0.035$ and $\delta\eta < 0.06$ between the track and the cluster.

The results are summarized in figure 9.

4.3 Isolation Efficiency

We have evaluated the $ISO < 0.1$ cut efficiency by throwing cones in the W sample. The basic procedure is as follows:

1) throw 7 cones at the same η as the W muon, but at $\phi = \phi_\mu + (2\pi/7) * i$, where $1 \leq i \leq 7$;

2) throw out any cone overlapping the cone containing the muon;

3) throw out any cone within R=0.4 of back-to-back in ϕ with the W p_t;

For a cone we define $ISO = \sum_{0.4}(E_t - E_t^c)/p_t^\mu$, where E_t^c is the transverse energy in the tower at the center of the cone. The ISO distribution thus obtained is shown in figure 17. Results are listed in Table 5, varying the method and the selection cuts to estimate the systematic uncertainty.

A problem arises when trying to evaluate ε_{iso} for the W sample by using the Z sample, or vice versa. The problem is that the muon p_t spectra for W's and Z's are different, due to the larger Z mass and to the fact that Z's in our data are more central since we require both muons to have low η. Since ISO = Econe/p_t^μ the ISO distributions are therefore different, and so are the cut efficiencies. This is one reason why we recommend against ISO as a variable for muons (see footnote in section 2). Figures 18 and 19 illustrate this point. We expect Econe to be the same for W and Z events. In figure 18, the Econe distribution from throwing cones in W and in Z events are superimposed. 14 cones were thrown per event, 7 at $\eta = +0.45$ and 7 at $\eta = -0.45$, to increase statistics in the Z curve. Cones overlapping a muon or back-to-back with the boson p_t are not included in the plot (dash=W normalized to

Z). The distributions look very similar. To test our understanding we calculated ε_{iso} using Econe from the W's but p_t^μ from the Z's. Table 5 lists these results as well.

To check the above result, we also measure the ISO efficiency using a second method. In this method, we begin with with a sample of very clean W-candidates, taken from the isolated and non-isolated golden muon samples (CENTRAL_MUO_I and CENTRAL_MUO_II, [7]), and see how many fail the isolation cut. The clean W sample is selected with the following cuts:

- $p_t > 30$ GeV/c, $\not\!\!E_T > 30$ GeV;
- EM < 2 GeV, HAD < 6 GeV;
- $r\phi$-impact < 0.05 cm, Berge's ztest < 0.8 (see C$TRK:TVDIST);
- $|dx| < 1$ cm, $|dz| < 2.5$ cm, $|dx_{slope}| < 20$ mrad;
- Muon track lies in the fiducial region, FIDCMU=0 [10].

Again, the results are summarized in table 5.

4.4 ε_{CMUO}

The factor ε_{CMUO} allows for pattern recognition and chamber inefficiency, and also for the small number of muons that are predicted to hit the chambers in the monte carlo but actually scatter out in the data. Beginning with the 2056 cosmic ray events used in the trigger studies [27], we counted the number of tracks that FIDCMU said should hit the muon chambers [10], but failed to make a CMUO bank. 70 of the 2056 tracks in the sample extrapolated to the chambers but didn't make a valid stub/track match, implying $\varepsilon_{CMUO} = 0.966 \pm 0.004$. Of the 70 tracks, at most 8 were cases of a track projected to the chambers scattering out. The rest were clear cases of the stub failing a quality cut in the stub/track matching routine (C$MUO:CMLNK requires that stubs have hits lying within a 2 mm road in the transverse direction, this cut accounts for about half of the stub failures).

Muon drift distance timing is different for cosmic rays than for $p\bar{p}$ data, and at the time of this writing it is not clear if the stub quality failure rate observed in the cosmic ray data is valid for the W and Z sample. Hence we use the second leg of the Z events to find ε_{CMUO}. From the 35 Z's with both tracks projecting to the muon chambers, only 69 tracks had another leg passing the selection criteria of the sample used in the study of ε_{CMUO}. Of these 69 tracks only one track did not make a CMUO bank, giving $\varepsilon_{CMUO} = 98.6\left(^{+1.2}_{-3.3}\right)\%$. The track that failed was one that passed through the good chamber region, but no stub/track match was formed, as in the cosmics. The result is statistically consistent with the cosmic result and even if we find that the cosmic result is systematically reliable it will not affect our conclusions.

Procedure	Result
basic	6862/7017=0.978
basic, veto jets with $E_t > 10.$	5002/5060 = 0.989
basic, but assign random $\|\eta\| < 0.8$ to cone	7596/7781 = 0.976
basic, but require cone to have FIDCMU=0	5295/5420 = 0.977
basic, but require muon tower in cone to pass HAD,EM cut	6856/7009 = 0.978
basic, but allow cone to overlap p_t^W	8045/8282 = 0.971
basic, but require $p_t^\mu > 30$, $\not\!\!E_T > 30$	4121/4202 = 0.981
basic, but require $p_t^\mu > 35$, $\not\!\!E_T > 35$	2419/2457 = 0.985
from clean W's	600/612=0.980
from clean W's, drop dz and dx_{slope} cuts, loosen dx cut to 2 cm	777/792=0.981
from clean W's, tighten p_t^μ, $\not\!\!E_T$ cuts to 35 GeV	383/386=0.992
Same as above 3, but no jets with $E_t > 10$ GeV	440/441=0.998
	569/572=0.995
	288/288=1.0
Convolute Econe spectrum from W's with Z° p_t spectrum	0.986
Ditto, but no jets with $E_t > 10$ GeV	0.996
Final (ϵ_{iso})	0.98 ± 0.01
Final, no jets with $E_t > 10$ GeV	0.99 ± 0.01

Table 5: Summary of study of isolation cut efficiency.

4.5 Combining the Efficiencies

If the variables we cut on are correlated then the product of the single efficiencies is less than the 'true' efficiency. First, the HAD and EM efficiencies are measured as a single cut thus taking the correlation between these two variables into account [23]. The Cosmic-Ray data results agree with the $p\bar{p}$ data results for the HAD and EM efficiency showing that isolation has a small effect on the HAD and EM efficiency. Figure 20 shows that in the W sample there is no correlation between dx and the sum of the EM and HAD energy in the towers traversed by the muons. The dx efficiency is measured for CMUO's passing the central muon trigger, important because both the Level 1 trigger and dx depend on the drift distance measurement, so that the source of an inefficiency in one can easily cause problems in the other. The dx efficiency sample had all of the other cuts applied to the sample except the dx cut. Therefore any correlation of the dx efficiency to the other cuts should already be taken into account by this number. The only other efficiency left that may have a correlation not accounted for is the Isolation efficiency. The Isolation efficiency was studied by throwing cones in isolated W events. This measurement should be unaffected by any other muon

parameter since the cone measurement only uses the calorimetry. The isolation was also studied using a clean set of W's with a tight dx cut. If Isolation and dx were correlated the results from these two methods should vary. These two methods give the same result. Loosening the muon matching requirements on the clean W sample does not change the result. Any correlations between cuts are small and as such the total efficiency of all the cuts is just the product of the individual efficiencies.

We check the overall combined efficiency using the second muons from Z's. We make a Z sample without the $ISO < 0.1$ or $|dx| < 2$ cm cut on the 'golden' muon, leaving 123 instead of 117 events. We look at 40 Z events where both tracks extrapolate to the chamber fiducial region and have $65 < M_{\mu\mu} < 115$ GeV/c^2. In the 40 events, there are 72 muons which had another leg satisfying the selection criteria and are thus usable for a study of the combined efficiency of the trigger, $ISO < 0.1$ and $|dx| < 2$ cm cuts times ε_{CMUO}. The result is that 59/72 muons pass the cuts for a combined efficiency of $81.9\left(^{+4.7}_{-5.7}\right)\%$. This should be compared with the product $\varepsilon_{ISO} \cdot \varepsilon_{dx} \cdot \varepsilon_{CMUO} \cdot T = 84.4 \pm 4.1\%$ taken from table 4. The 1σ agreement between the product of the efficiencies and the meaured combined efficiency shows that correlations are not a problem.

5 Backgrounds

Type of Background	Events
Backgrounds to W	
QCD	30 ± 20
$Z \to \mu\mu$	$140 \pm 13 \pm 5$
$W \to \tau\nu$	$49 \pm 2 \pm 9$
$Z \to \tau\tau$	$3 \pm 0.3 \pm 0.9$
Top	$0^{+15.2}_{-0}$
Cosmics	6 ± 3
Backgrounds to Z	
$Z \to \tau\tau$	0^{+1}_{-0}
$W+$ jet	0^{+1}_{-0}
QCD	0^{+1}_{-0}
Drell-Yan	0^{+1}_{-0}
Cosmics	0.4 ± 0.4
Total W background	$B_W = 228^{+41}_{-26}$
Total Z background	$B_Z = 0.4 \pm 1$

Table 6: Backgrounds.

Table 6 lists the important backgrounds to the W and Z signals. The Z's are

essentially background-free. The biggest W backgrounds are

i) $Z^\circ \to \mu^+\mu^-$ where one muon is undetected;

ii) $W \to \tau\nu$, $\tau \to \mu X$;

iii) QCD dijets faking a muon and large $\not\!\!E_{\rm T}$.

In this section we describe how we estimated these backgrounds as well as some smaller ones.

5.1 Backgrounds from non-Signal W's and Z's

The largest W background is $Z^\circ \to \mu^+\mu^-$ events where one muon hits the chambers and the other is unobserved. We estimate this rate by calculating our acceptance for these events in the same way as for the detected Z's (A_{WZ}, see table 1). We then take the number of observed Z's, correct for efficiencies, and predict the number with a missing second muon. We expect 140 such events in our W sample, with a statistical error of 13 events, and a systematic error due to structure functions and the Z p_t spectrum of ± 5 events. As a cross-check we used ISAJET to obtain 137 ± 10 events.

ISAJET also generates $Z^\circ \to \tau\tau$ and $W \to \tau\nu$ events. These are passed through CDFSIM. We calculate acceptances from ISAJET in a similar manner to the A_{00} and A_{0X} calculation. Backgrounds from $Z^\circ \to \tau\tau$ and $W \to \tau\nu$ are normalized to data and are therefore independent of the boson cross-sections in the Monte Carlo.

Finally, in our W sample we observe 6 Z-candidate events, that is, dimuon pairs with $65 < M_{\mu\mu} < 115$ GeV but where the second muon fails the muon tower energy cuts. The rate is consistent with our measured efficiencies. We explicitly remove these events from the sample.[2]

5.2 QCD backgrounds

The production cross section for dijets having $E_t > 20$ GeV in the region $|\eta| < 0.6$ is around 600 nb, or 300 times bigger than the $W \to \mu\nu$ rate. Even with a low probability of a jet fragmenting into a stiff isolated particle, and that particle then faking a muon, while the balancing jet is somehow lost in the calorimeter making large missing energy, dijets faking stiff leptons turn out to be a large background to $W \to \mu\nu$. Dijets could also contribute to the $Z^\circ \to \mu^+\mu^-$ background, where the same process of a jet fluctuating to a muon candidate could cause a $W+$ jet event to look like a Z.

Also, the $b\bar{b}$ production cross-section at CDF is $8.5 \pm 4.3\mu b$ for $p_t^b > 10$ GeV, in the central region [31]. About 37% of b's decay to a real muon, either through semi-leptonic decay or via decay to charm and subsequent muonic charm decay. There will be a (soft)

[2]The measured efficiency of the muon tower energy cut using second legs of Z's is 95.2+1.8-2.5 %. The measured efficiency using J/ψ's is 98.7 $\pm$ 0.28. These are consistent at the 2 σ level.

neutrino in the event. The other b can make a mismeasured jet and hence contribute to $\not\!\!E_T$ in the event. This also makes $W \to \mu\nu$ background.

5.2.1 DiJet Background in $W \to \mu\nu$: The Electron Method

We follow the electron example [3]. Figure 21 illustrates the basic point. The plot shows the $\not\!\!E_T$ distribution for events with isolated golden muons (dash histogram). ($\not\!\!E_T$ is the calorimeter missing E_t corrected for the muon p_t and for the muon energy deposition, see equation (11) and reference [7].) The distribution is falling at low momenta, characteristic of jet events, until the turn-on of the W Jacobian at higher $\not\!\!E_T$. We select W events by requiring $\not\!\!E_T > 20$ GeV. But it is clear from the plot that the a remnant of the falling background continues under the Jacobian.

The obvious approach is to fit the background at low $\not\!\!E_T$, and extrapolate to the W region. The problem is that W events contaminate the background spectrum even at low $\not\!\!E_T$, affecting the shape in an unknown way. More importantly, mis-reconstructed tracks (for example, from pion and kaon decay-in-flight) distort the large missing E_t spectrum. A solution is to take a background sample with the same shape, and scale appropriately. This is shown with the solid histogram in figure 21, which has the same cuts except requiring ISO > 0.3 instead of ISO < 0.1 as for the dashed curve. The background sample requires a jet (favoring QCD events) and a non-isolated muon (rejecting W events). Z's are explicitly vetoed.

The method assumes that for the background events, ISO and $\not\!\!E_T$ are uncorrelated. Non-correlation is plausible: dijet events come from $q\bar{q}$ or gluon-gluon scattering with subsequent hadronization and fragmentation. Once the parton pair has been produced, the two partons evolve independently. The $W \to \mu\nu$ background events would be those where one parton happened to fluctuate into an isolated muon candidate, and the other parton fragmented into particles lost into the detector cracks or the beampipe. Figure 22 shows how the isolation distribution evolves with missing E_t. ISO is plotted for four $\not\!\!E_T$ bins, $0 < \not\!\!E_T < 5$, $5 < \not\!\!E_T < 10$, $10 < \not\!\!E_T < 15$, and $15 < \not\!\!E_T < 20$, requiring the jet in the background sample to have $E_t > 10$. The shape of the ISO distribution changes somewhat with $\not\!\!E_T$. For $\not\!\!E_T > 20$ GeV, W contamination in the background plot makes it difficult to see what happens to ISO.

ISO and $\not\!\!E_T$ would be strongly correlated if the energy lost in cracks made the muon-candidate appear isolated at the same time that $\not\!\!E_T$ is produced. There is also a strong correlation if large $\not\!\!E_T$ comes from p_t overestimates for poorly reconstructed tracks, because ISO is artificially decreased because $ISO \equiv BTE/p_t$, The variation in figure 22 is small enough that we proceed with the method, and assign an uncertainty large enough to allow for the correlation. We calculate the number of background events in the W sample as follows: In figure 21,
the number of events on the dashed curve at low p_t^ν is 'a',
the number of events on the solid curve at low p_t^ν is 'b', and

Cut	$\|dx\| < 2$ cm	$\|dx\| < 10$ cm
No jet req't	20-26 events	29-40 events
≥ 1 10 GeV jet	17-24	29-37
≥ 1 20 GeV jet	7-15	16-24
≥ 2 10 GeV jet	6	11

Table 7: QCD background estimate for the ISO and $\not\!\!E_T$ method for different control sample definitions.

the number of events on the solid curve at high p_t^ν is 'c'.
Restated,

'a' is the events with ISO< 0.1, and $\not\!\!E_T < 10$;

'b' is the events with ISO> 0.3, and $\not\!\!E_T < 10$, and a jet $E_t > 10$;

'c' is the events with ISO> 0.3, and $\not\!\!E_T > 10$, and a jet $E_t > 10$;

so the number of background events in the W region is

$$bgrd = a/b * c.$$

The number N_W of W candidates is those events with ISO < 0.1 and $p_t^\nu > 20$ so that the background fraction is $bgrd/N_W$.

Parameters can be varied in the above approach. The jet and isolation cuts defining the background sample, for example, or the $\not\!\!E_T$ cut defining the low $\not\!\!E_T$ region. Vetoing jets cleans up the W sample significantly, as was done in the first electron analysis. Figure 23 shows the the jet multiplicity of the $W \rightarrow \mu\nu$ sample. Table 7 summarizes some results. We have observed that for dijet-like events, the background tends to be underestimated, hence we favor the larger values. That is, we know that requiring jets leads us to underestimate the background, so to be conservative we pick the upper end of the range in table 7 and assign a symmetric error bar. From this analysis we conclude 30 ± 20 background events.

5.2.2 Jet-muon angle method

The shortcoming of the above method is the unknown relation between $\not\!\!E_T$ and ISO. Hence we try an approach using other variables. $\Delta\phi_{\mu j}$, the azimuth angle between the muon and the highest E_t jet in the event, is well predicted by the Monte Carlo, and we expect the distribution to be different than for the background. Jets must have $E_t > 10$ GeV. We used Papageno $W + 1$ and $W + 2$ jet events, and electron data events, to compare with the distribution from the muon data. The distributions for the 1 and 2 jet monte carlo are similar, so that weighting the different diagrams in proper proportion is not a concern. We have reproduced the similar plots in [30], hence seem to be using the Monte Carlo properly. The muon data agrees nicely with the electron data, except that the electron data has an excess in the back-to-back bin that is not apparent in the muon data. (The electron excess is

consistent with a 2 sigma statistical fluctuation, or with 50 background events. The electron analysis found 100 ± 50 background events in their 2664 W-candidates).

W+jet data is sloped in $\Delta\phi_{\mu j}$, favoring jets back-to-back with the muon, as seen in figure 24. The background, on the other hand peaks at 180° and somewhat at 0°, with almost nothing in between, as in figure 25 (no ISO cut). The muon data agrees nicely with the monte carlo (normalized to the number of muon+jet events). The apparent excess near $\Delta\phi_{\mu j} = 0$ could be an artifact of the fact that both Papageno and the jet algorithm suppress jets within $dR = 0.8$ of another cluster. In figure 26 that same cut is applied the muon data, again overlayed with Papageno. The agreement is very good.

Taking figure 26 at face value, the muon QCD background is small. Taking figure 24 at face value, the QCD background is the excess in the first bins, or 20 events. Hence this analysis is consistent with the earlier estimate of 30 ± 20 background events in the W sample.

5.2.3 DiJet Background in $Z^\circ \rightarrow \mu^+\mu^-$

In the case of the dijet background to the $W \rightarrow \mu\nu$ sample, one jet fluctuated to look like a muon while the second jet fluctuated to produce significant $\not\!\!E_T$. In principle Z's are simpler: both jets fluctuate to an isolated fake muon. That we see no like sign muon pairs in the Z mass region suggests that this background to the Z's is small. If we attempt to calculate the background following the electron analysis, as described in [3], we find no events with large ISO (background region) and so we can't extrapolate to low ISO (signal region), confirming the impression that there is no background.

In an independent study, we count events in the CENTRAL_MUO_I, II data sample with 1 gold muon and an additional track with $p_t > 20$ that *fails* the minimum ionizing cuts, i.e., the track has $E^{EM} > 2$ or $E_{had} > 6$. The idea is that a second track failing the minimum ionizing cuts is a pion, and then we use the known punchthrough probability to estimate how many of the second tracks could fake a muon. Non-interacting punchthrough probability is certainly less than 1/50 [16].

There are 34 such events, of which 16 have opposite charge, of which 12 have invariant mass in the range 65-115 GeV/c^2. If, in addition, the track must fail the minimum ionizing cut by a large margin, there are even fewer events. For example $E^{EM} + E^{had} > 10$ GeV gives 8 events in the 65-115 mass region. Multiplying by the punchthrough probability predicts < 1 QCD background event in the Z sample.

5.3 Cosmic Rays

Removal of cosmic rays from the W and Z sample is described in detail in [15]. Briefly, reconstruction of the cosmic ray track as it goes towards the CTC center is generally worse than for tracks emanating from the center, because the time-of-flight corrections are wrong. Also, most cosmics do not pass directly through the event vertex. Hence looking for a

poor quality track back-to-back with the muon candidate rejects the majority of cosmic rays. Track quality is determined from the impact parameter in the $r\phi$- and rz-planes, and from the fraction of hits and segments used in the track. A small number of events have a high-quality track that is back-to-back with the muon candidate, in both η and ϕ, that passes through the vertex. In these cases CTC timing information determines whether the two tracks, fitted as a single particle, are consistent with separate particles coming from the vertex, or a single particle passing through the detector. Only a few events are judged by this criterion. The filter efficiency for our events, and the number of cosmic ray events remaining in the sample, come from scanning and from applying the filter to electron data. For W events, we found $99.8^{+0.1}_{-0.2}\%$ efficiency, while for Z events we found $99.6^{+0.3}_{-1.0}\%$. We combined the two results to obtain the value in table 4. Background estimates are listed in table 6.

5.4 Top Backgrounds

If the Top quark is more massive than the W boson then Top mesons will decay into real W's, creating a background. The predicted cross section for $\sigma(p\bar{p} \rightarrow t\bar{t})$ at CDF energies is 150 pb^{-1}, if the top quark mass is at the present CDF limit of 90 GeV. We ran ISAJET with CDFSIM and then applied our standard $W \rightarrow \mu\nu$ event selection and found that 15 events would be in our W sample if $M_{top} = 90$ GeV. Since the cross section is falling with increasing Top mass this is an upper bound on the Top background.

6 Results

Dimuon pairs are produced from quark-antiquark annihilation into (virtual) photons and Z's, so that the cross section is a combination of three terms,

$$\sigma(p\bar{p} \rightarrow \mu\mu) = Z^2 + \gamma Z + \gamma^2$$

where γZ represents the interference terms between the pure Z process and the pure γ process. In the mass window $65 < M_{\mu\mu} < 115$ dimuons come mainly from the Z term, although the photon terms contribute. Theorists usually neglect the photon terms in their calculations and assume that the finite Z width has a negligible effect on the total cross section, so to compare with theory we need to correct for these contributions to the rate.

We calculate the correction using the latest version of the Toy monte carlo that includes the photon terms to calculate the cross sections, as well as with ISAJET, by computing the two factors

$$I_1 = \int_{50}^{150} Z^2 dM$$

$$I_2 = \int_{65}^{115} (Z^2 + \gamma Z + \gamma^2) dM$$

	$W \to \mu\nu$	$W \to e\nu$
Candidates	1431	2664
Background	228^{+41}_{-26}	238^{+62}_{-53}
Signal	$1203 \pm 38^{+26}_{-41}$	$2426 \pm 52^{+53}_{-62}$
Acceptance	$18.14 \pm 0.12 \pm 0.65\%$	$32.1 \pm 1.5\%$
Efficiency	$90 \pm 1\%$	$84 \pm 3\%$
Trigger	$91 \pm 2\%$	$98 \pm 1\%$
Luminosity	$3.54 \pm 0.24\ pb^{-1}$	$4.05 \pm 0.28\ pb^{-1}$
Cross Section	$2.29 \pm 0.07 \pm 0.20\ nb$	$2.19 \pm 0.04 \pm 0.21\ nb$
	$Z^\circ \to \mu^+\mu^-$	$Z^\circ \to e^+e^-$
Candidates	108	243
Background	0.4 ± 1	5 ± 3
Signal	$107 \pm 10 \pm 1$	$238 \pm 16 \pm 3$
Acceptance	$A_{00} = 4.57 \pm 0.07 \pm 0.15\%$	Total=$35.2 \pm 0.6\%$
	$A_{0X} = 10.42 \pm 0.10 \pm 0.25\%$	
2^{nd} Leg Efficiency	$97.4 \pm 1.0\%$	$92 \pm 3\%$
Luminosity	$3.54 \pm 0.24 pb^{-1}$	$4.05 \pm 0.28 pb^{-1}$
Cross Section	$0.238 \pm 0.023 \pm 0.18\ nb$	$0.209 \pm 0.013 \pm 0.017\ nb$

Table 8: Results for muon and electron analyses.

and find that $I_1/I_2 = 0.99$. Both monte carlos agree to within 0.2%. This is not strictly the correct way to make the correction, but gives a feel for the magnitude of the effect. We multiply our final Z cross section by this factor.

Armed with equations 3 to 7 and table 8, calculating the cross-sections and R_μ is simple. We obtain

$$\sigma(W \to \mu\nu) = 2290 \pm 73\ (stat) \pm 120\ (sys) \pm 150\ (lum)\ pb.$$

Similarly,

$$\sigma(Z^\circ \to \mu^+\mu^-) = 238 \pm 23\ (stat) \pm 9\ (sys) \pm 16\ (lum)\ pb$$

where the first error term is statistical, the second is due to systematic uncertainties in the acceptance and efficiencies and the last term comes from the luminosity measurement. The cross-section ratio is

$$R_\mu = 9.6\ \pm\ 1.1\ (stat)\ \pm\ 0.5\ (sys)$$

7 No-jet Analysis

Repeating the cross-section analysis for a data subset without jets provides a check on our work. QCD and tau backgrounds are smaller, allowing for a potentially smaller systematic error bar, although at a cost in statistics. Changed acceptances, due to the different boson p_t spectrum and smaller contributions from higher order diagrams, test the robustness of the final result.

After vetoing events having a JETS bank with $\sqrt{\mathrm{EJET}^2 - \mathrm{PZJET}^2} > 10$ GeV we find 1011 W- and 72 Z-candidates. Table 9 lists the factors for the no-jet measurement (factors not listed are the same as before). These come from repeating the studies described throughout this note for the no-jet sample. For example, the acceptances are recalculated using boson p_t spectra and the $\sum E_t$ distribution for the underlying event taken from no-jet data. The Z acceptances are about 10% smaller in the no-jet case, mainly because low p_t Z's are less central. On the other hand, the W acceptance is almost unchanged, because the effect of lower W p_t is offset by reduced $\not\!\!E_T$ smearing.

Figure 27 shows that the QCD background in the no-jet sample is close to zero. 12 events have $\not\!\!E_T > 20$ and $ISO > 0.1$ which agrees with the no-jet result $\epsilon_{ISO} = 99 \pm 1\%$ listed in table 5.

To compare the no-jet answer with our previous result, R must be decreased by a factor 1.008 ± 0.005, since the jet veto biases the data towards lower-order diagrams. The correction was calculated by Stirling et al [32]. In the end we get

$$R_\mu = 9.93\ \pm\ 1.3\ (stat)\ \pm\ 0.4\ (sys)$$

using the no-jet analysis.

Factor	Value
W Candidates	1011 events
Z Candidates	72 events
QCD W Background	0 ± 5 events
One-legged Z background	$99 \pm 12 \pm 3$ events
$W \rightarrow \tau\nu$ W background	$31 \pm 1 \pm 5$ events
$Z^\circ \rightarrow \tau\tau$ W background	$1 \pm .1 \pm .3$ events
W cosmic background	4 ± 1 events
A_W	$18.35 \pm 0.12 \pm 0.63\%$
A_{00}	$4.52 \pm 0.07 \pm 0.23\%$
A_{0X}	$10.06 \pm 0.10 \pm 0.47\%$
A_{ZW}	$20.50 \pm 0.13 \pm 0.66\%$
'raw' R	$10.0 \pm 1.3 \pm 0.4$
Higher order correction	1.008 ± 0.005
R	$9.93 \pm 1.3 \pm 0.4$

Table 9: Values for the no-jet measurement.

8 Comparison with Standard Model Parameters

Figure 28 superimposes our cross-section results on the theoretical prediction [33].

If the Top quark is lighter than the W boson, the decay $W \rightarrow t\bar{b}$ is possible. The decay rate $\Gamma(W \rightarrow \mu\nu)$ depends on the Top mass, according to the phase space available to daughter Top quarks. Re-arranging equation 2 yields

$$\frac{\Gamma(W \rightarrow \mu\nu)}{\Gamma(W)} = R \times \frac{\sigma(Z)}{\sigma(W)} \times \frac{\Gamma(Z^\circ \rightarrow \mu^+\mu^-)}{\Gamma(Z^\circ)}$$

Theoretical uncertainties largely cancel in the total cross-section ratio, giving

$$\frac{\sigma(p\bar{p} \rightarrow WX)}{\sigma(p\bar{p} \rightarrow ZX)} = 3.23 \pm 0.03$$

at $\sqrt{s} = 1.8$ TeV [32], and the Z total and partial widths have been measured at LEP, $\Gamma(Z^\circ \rightarrow \mu^+\mu^-) = 83.3 \pm 0.9$ MeV and $\Gamma(Z^\circ) = 2.487 \pm 0.009$ GeV [35]. Combining, we obtain

$$BR(W \rightarrow \mu\nu) = \frac{\Gamma(W \rightarrow \mu\nu)}{\Gamma(W)} = 0.100 \pm 0.012$$

which is superimposed on the theoretical Top mass dependent curve in Figure 29. At the 95% Confidence Level we can not place a limit on Top quark mass.

When CDF first measured R in the electron channel, R gave the best Top limit because the 15% luminosity uncertainty canceled in the cross-section ratio and because the

$Z^\circ \to e^+e^-$ statistics are adequate. But the error on R_μ is dominated by the $Z^\circ \to \mu^+\mu^-$ statistics, and the luminosity error has been halved. Hence, adequate results come from

$$\frac{\Gamma(W \to \mu\nu)}{\Gamma(W)} = \frac{\sigma(W \to \mu\nu)}{\sigma(W)},$$

where $\sigma(W) = 19.8$ nb [34]. A 14% error on $\sigma(W)$ dominates the uncertainty, due mainly to $\mathcal{O}(\alpha^3)$ corrections. The result in this case is

$$BR(W \to \mu\nu) = \frac{\Gamma(W \to \mu\nu)}{\Gamma(W)} = 0.12 \pm 0.02,$$

and using the particle data group [36] method for a physically bounded region this yields the same 90% C.L. on the branching ratio as we obtained with R. If higher-order corrections are improved before we increase our $Z^\circ \to \mu^+\mu^-$ statistics, this method could give a better Top mass limit.

The total width $\Gamma(W)$ of the W also depends on R. Rearranging equation 2 yet again gives

$$\frac{\Gamma(W)}{\Gamma(Z)} = \frac{1}{R}\frac{\sigma(W)}{\sigma(Z)}\frac{\Gamma(W \to \mu\nu)}{\Gamma(Z^\circ \to \mu^+\mu^-)},$$

and taking the theoretical value $\Gamma(W \to \mu\nu)/\Gamma(Z^\circ \to \mu^+\mu^-) = 2.70 \pm 0.02$ we obtain $\Gamma(W)/\Gamma(Z) = 0.91 \pm 0.12$, and $\Gamma(W) = 2.27 \pm 0.30$ GeV, where we have again used the LEP results mentioned above. This number agrees with the electron result, $\Gamma(W) = 2.12 \pm 0.20$ and with the theoretical prediction of 2.07.

Acknowledgements

We'd like to thank the several people who helped us in this analysis. In particular, Tom Westhusing for blazing the muon R trail; Paul Derwent and Claudio Campagnari and Marshall Miller for blazing the R trail with electrons; Aesook Byon-Wagner for the painstaking data sample preparation; Leigh Markosky for the Z QCD background; Cathy Newman-Holmes for her W QCD background help; Carla Grosso-Pilcher for evaluating the Top background for us; and most certainly Steve Errede and Henry Frisch for their unflagging support & encouragement.

Appendix A: Flow Chart of Cone Energy Routine

This is a "flow chart" showing how BTE is calculated in the present muon analysis code.

- Initialize Geometry
  - get inner and outer radius of CEM
  - get inner and outer radius of CHA
  - get start/stop angles for each eta wedge
  - get start/stop Z positions for each eta wedge
    - at inner CEM
    - at outer CEM
    - at inner CHA
    - at outer CHA
- Fudge SETA, EVTA
  - look for EVTA (Z event vertex)
  - if cannot find
    - store SETA in TEMP ($\sin\theta$ of each wedge)
    - create EVTA using Z0 of track
    - make SETA from new EVTA
    - drop new EVTA
  - otherwise
    - store event vertex in variable ZVTX
    - if event vertex is more than 1 cm from Z0 of track
      - alter EVTA so it contains Z0 of track
      - store SETA in TEMP
      - remake SETA with new EVTA
- Propagate track
  - propagate track to inner CEM, assuming straight trajectory and store Z of track at inner CEM in ZTRP(1)
  - propagate track to outer CEM, assuming straight trajectory and store Z of track at outer CEM in ZTRP(2)
  - propagate track to inner CHA,assuming straight trajectory and store Z of track at inner CHA in ZTRP(3)

- propagate track to outer CHA,assuming straight trajectory and store Z of track at outer CHA in ZTRP(4)
- using ZTRP, find eta annulus muon is in at
  * inner CEM (ICEMI)
  * outer CEM (ICEMO)
  * inner CHA (ICHAI)
  * outer CHA (ICHAO)

- Get Muon Tower Energy
  - if in central at all 4 points
    * get em energy of muon tower
      · find TOWE
      · find SETA
      · get phi of muon track at origin
      · for all eta annuli mu crosses (ICEMI to ICEMO, or vice versa), get E from TOWE for tower at muon track phi and $E_t = E \sin\theta$ from SETA
    * get had energy of muon tower
  - otherwise: (we don't care about this case, I think...)

- Get Total Cone Energy

  call CMCONE - documented below - and get total cone Et

- Finish
  - BTE=total cone Et - mu tower Et
  - remake EVTA
  - remake SETA

Appendix B: CMCONE flow chart

- Find TOWE
- Find SETA
- For HAD
  - find eta annuli where abs(eta_annuli - eta_track) is minimum, where eta_annuli comes from SETA
  - call this OLETA
  - find largest (in 1-84 sense) eta annuli where eta_annuli - eta_track is less or equal to the cone size
  - call this IIMAX
  - find smallest (in 1-84 sense) eta annuli where eta_track-eta_annuli is less than or equal to the cone size
  - call this IIMIN
  - For eta annuli IIMIN to IIMAX, loop over phi towers in that annulus
    * get TOWE data for this tower
    * calculate deltaphi =largest delta phi can be for this annuli and still be within the cone = sqrt(cone size**2 - (eta_annuli-eta_track)**2)
    * if cone size is very small, bump delta phi up to .131
    * find phi of this phi tower, phi_tower
    * if cone size is very small, and we are in a central thru plug/wall overlap annulus, kludge phi_tower
    * if cos(phi_tower-phi_track) $\geq \cos \delta\phi$, SUM energy in tower * $\sin\theta$ as stored in SETA
- repeat for EM

References

[1] F. Abe et al., *Measurement of the Ratio* $\sigma(W \to e\nu)/\sigma(Z^\circ \to e^+e^-)$ *in* $p\bar{p}$ *Collisions at* $\sqrt{s} = 1.8$ *TeV*, Phys. Rev. Lett. **64** 152 (1990).

[2] F. Abe et al., *A Measurement of* $\sigma \cdot B(W \to e\nu)$ *and* $\sigma \cdot B(Z^\circ \to e^+e^-)$ *in* $p\bar{p}$ *Collisions at* $\sqrt{s} = 1800$ *GeV*, submitted to Phys. Rev. D.

[3] P. Derwent et al., *Measurement of* $\sigma(W \to e\nu)$ *and* $\sigma(Z^\circ \to e^+e^-)$ *in* $p\bar{p}$ *Collisions at* $\sqrt{s} = 1.8$ *TeV*, **CDF-1107.**

[4] P. Derwent et al., *Checks for the W and Z° Cross Section Measurement*, **CDF-1254.**

[5] T.M. Liss, *GMUFLT: The Muon Filter in Production*, **CDF-1080.**

[6] R. Swartz and D. Kardelis, *The Making of a Muon Sample*, **CDF-1220.**

[7] A. Byon et al., *A Standard Data Sample for the* $W \to \mu\nu$ *and* $Z^\circ \to \mu^+\mu^-$ *Analysis*, **CDF-1263.**

[8] T.K. Westhusing, *The Central Muon Analysis Code*, **CDF-737.**

[9] P. Derwent and M. Miller, *A Standard Data Sample for* $W \to e\nu$ *and* $Z^\circ \to e^+e^-$ *Analysis*, **CDF-1166**

[10] D.A. Smith and R.L. Swartz, *Fiducial Cuts for Central Muons*, **CDF-1259.**

[11] M. Miller, *Fiducial Cuts for Electrons*, **CDF-1086.**

[12] T.K. Westhusing and H. Grassmann, $Z^\circ \to \mu^+\mu^-$*: Efficiency of the Pseudorapidity Cuts and Track Reconstruction*, **CDF-1012.**

[13] M. Gold, *Search for High Mass Electron Pairs*, **CDF-1229**
M. Gold, *Limits on Z' and Compositeness from* $p\bar{p} \to e^+e^-X$, **CDF-1302.**

[14] A. Byon thesis (Purdue University), page 67.

[15] A. Byon et al., *Cosmic Filtering of Central Muon Events*, **CDF-1260.**

[16] D.A. Smith and H.B. Jensen, *Pion Punchthrough Probability in the Central Calorimeter*, **CDF-707,**
B. Denby, *A New Look at Punchthrough at CDF*, **CDF-1324.**

[17] S. Edner et al., *Search for* $W' \to \mu\nu$, **CDF-1279.**

[18] C. Campagnari, *A Fast W and Z Monte Carlo*, **CDF-1025.**

[19] R. Hamberg et al., *A complete calculation of the order α_s^2 correction to the Drell Yan K-Factor*, Desy 90-129,October 1990.

[20] F. Abe et al, *A Measurement of the W Boson Mass in 1.8 TeV $\bar{p}p$ Collisions*, submitted to Phys. Rev. D.
P. Schlabach, PhD. Thesis, University of Illinois at Urbana-Champaign (1990)

[21] B. Winer and P. Tipton, *The W Boson Differential Cross Section, $\frac{d\sigma}{dp_t}$*, **CDF-1287.**

[22] Johnny Ng et al, *Measurement of the $Z^\circ \rightarrow \mu^+\mu^-$ $d\sigma/dp_t$*, **CDF-1323**;
Johnny Ng et al, *Some Details in the Muon Analysis for the $d\sigma/dp_t$ Measurement*, **CDF-1342.**

[23] D. Kardelis, *Efficiency of the "Standard" Muon Tower Calorimeter Cuts for W/Z Muon Analysis*, **CDF-1301.**

[24] D. Kardelis, *A Study of the CTC-CMU Matching Cut Efficiency for W/Z Muon Analysis*, **CDF-1336.**

[25] C. Grosso-Pilcher and S. White, *CDF Luminosity Calibration*, **CDF-1202.**

[26] A. Gauthier, *Milestones of the Central Muon Trigger*, **CDF-1029.**

[27] A. Gauthier, *Efficiency of the Level 1 Central Muon Trigger*, **CDF-937.**

[28] A. Gauthier and D. Kardelis, *Efficiency of the Level 2 Central Muon Trigger*, **CDF-1106.**

[29] A. Gauthier, *Efficiency of the Level 3 Central Muon Trigger*, **CDF-1145.**

[30] P. Sinervo and J. Walsh, *Comparison of e+jets with W+jets Monte Carlo*, **CDF-932.**

[31] R. Hughes et al, *Measuring the b quark cross section using the exclusive decays*, **CDF-1382.**

[32] A.D. Martin, W.J. Stirling, and R.G. Roberts, Phys. Lett. **228B**, 149 (1989).

[33] Altarelli, Ellis, Greco, and Martinelli, Nucl. Phys. **246B**, 12 (1984)
Altarelli, Ellis, and Martinelli, Z. Phys. **27C**, 617 (1985).

[34] R.K. Ellis, in proceedings of the 8th Topical Workshop on $p\bar{p}$ Physics, Castiglione, September 1989,
and also in Fermilab-Conf-90/45-T.

[35] S. L. Lloyd, in proceedings of the Aspen Winter Conference, January 1991. Same values were also presented at Moriond, March 1991.

[36] Particle Data Group, *Review of Particle Properties*, Phys. Lett. **239B**, III.35 (April 1990).

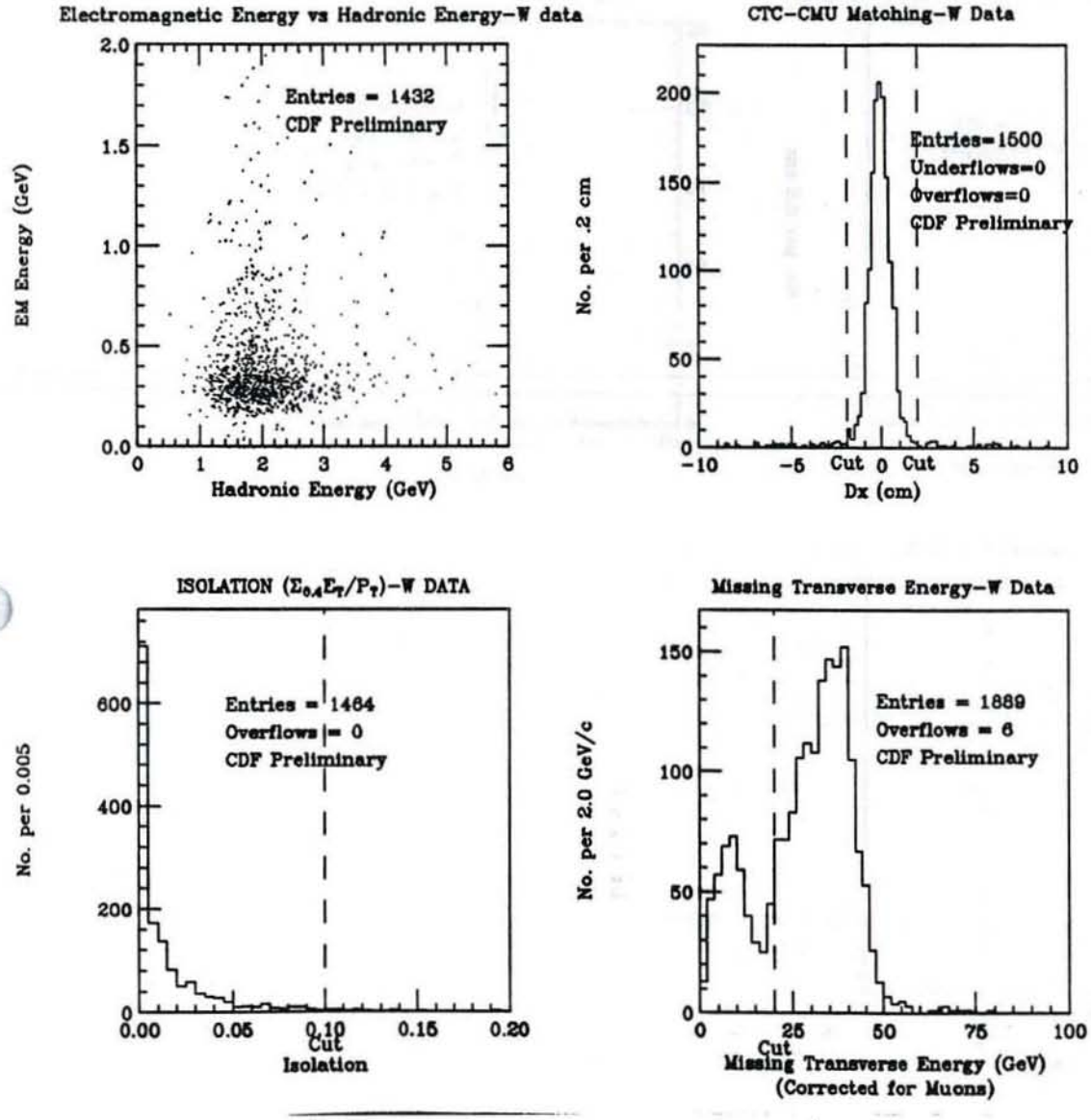

Figure 1: Variables used to define the W sample.

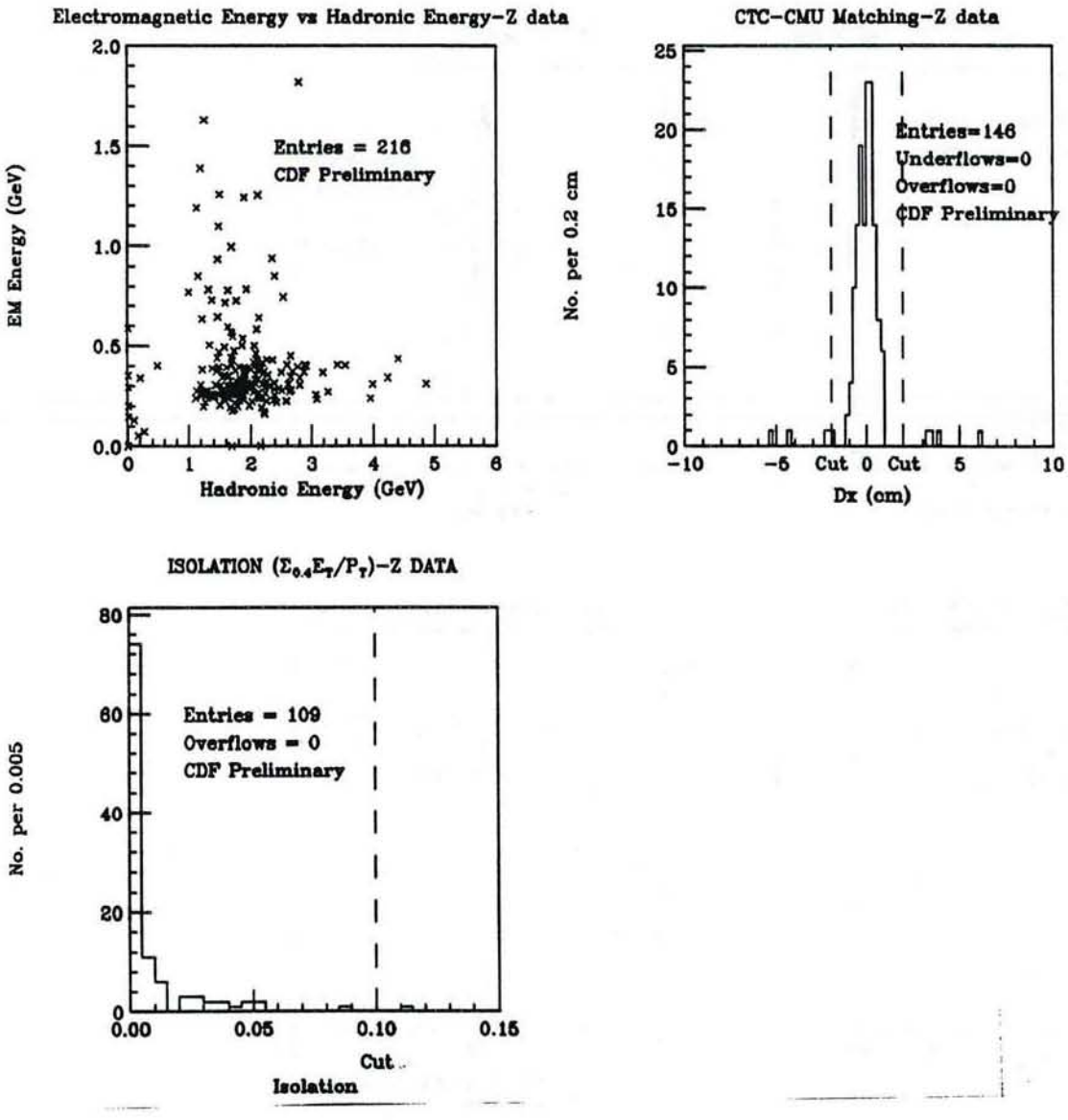

Figure 2: Variables used to define Z^o sample.

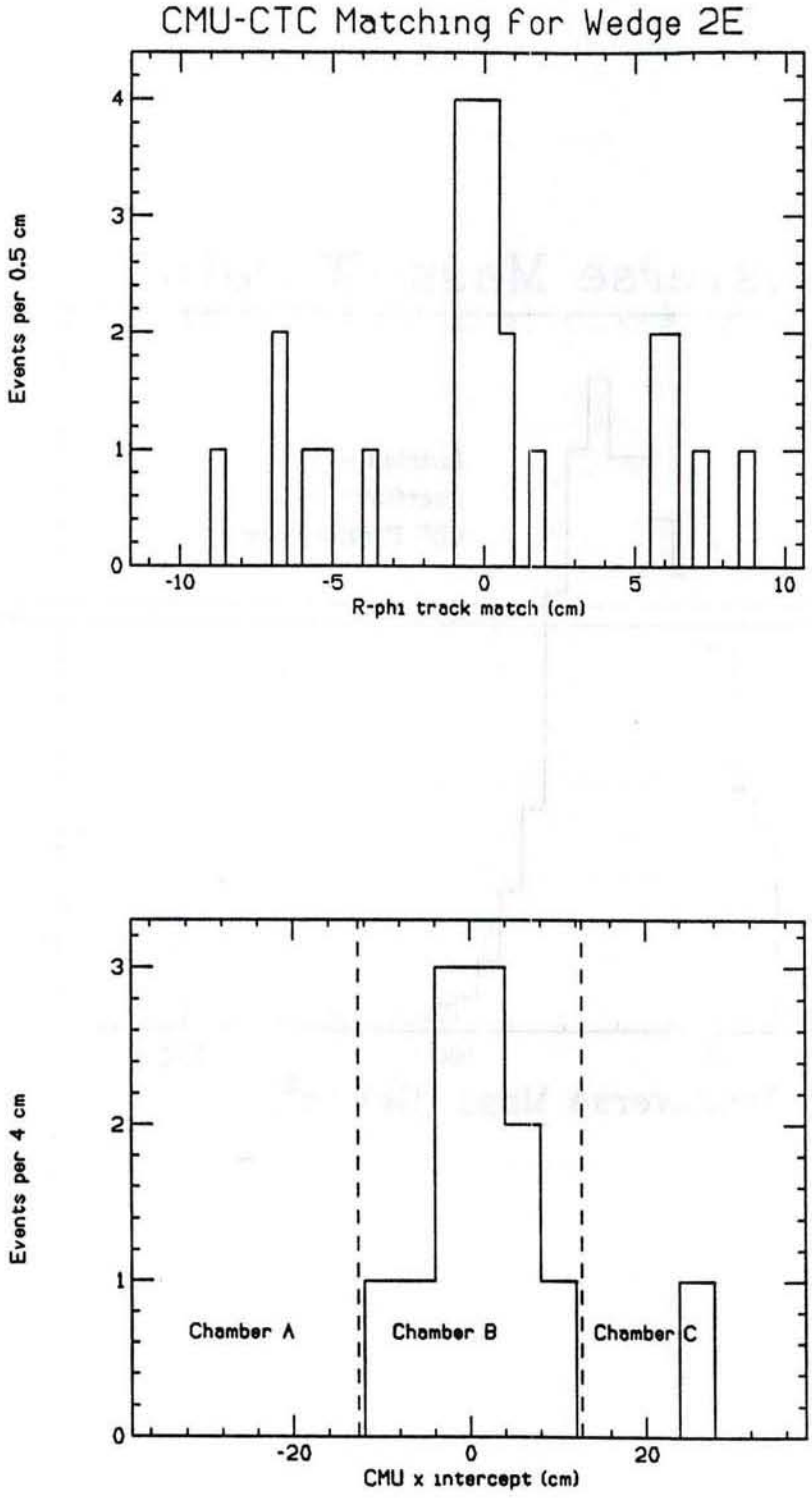

Figure 3: CMU-CTC track match variables in $r\phi$-plane for wedge 2E. Top shows difference between CTC track extrapolated to muon chambers and measured muon stub position, dx, as in figure 1b. Bottom shows stub intercept position for tracks that failed the dx cut in wedge 2E.

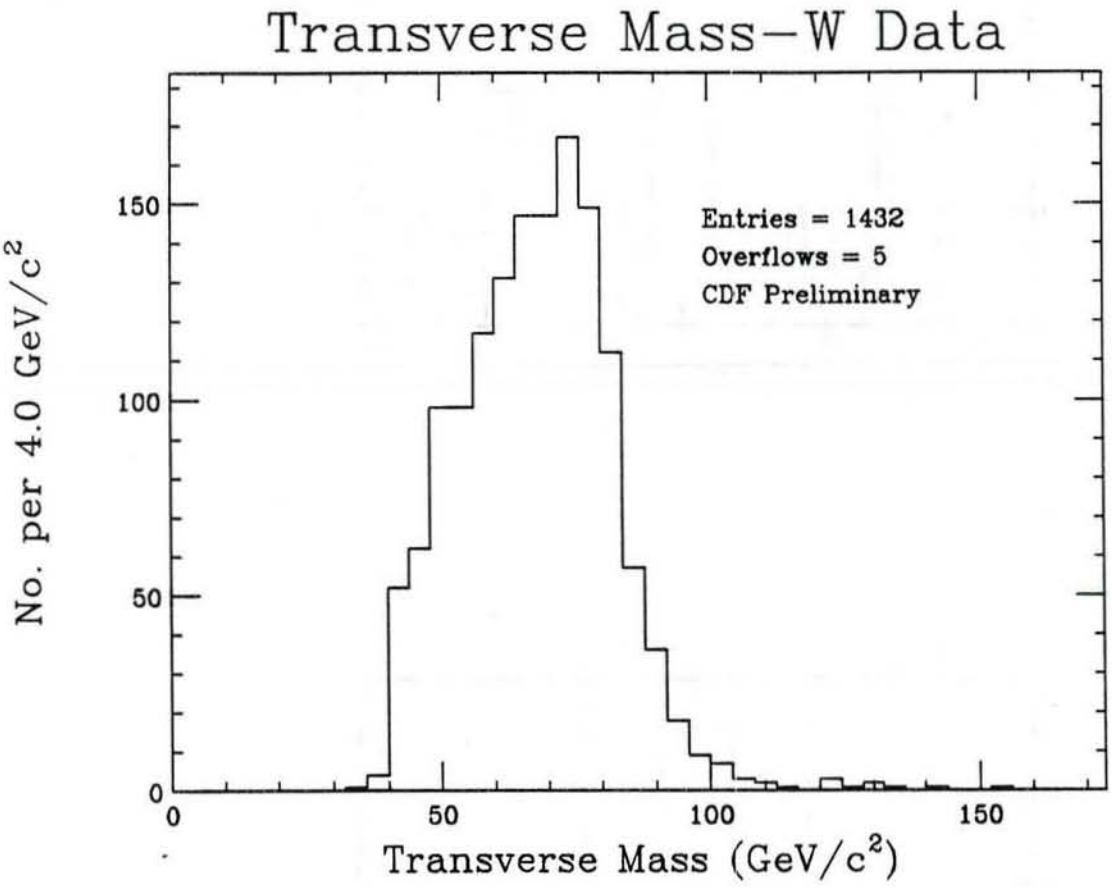

Figure 4: Transverse mass distribution for the $W \rightarrow \mu\nu$ sample.

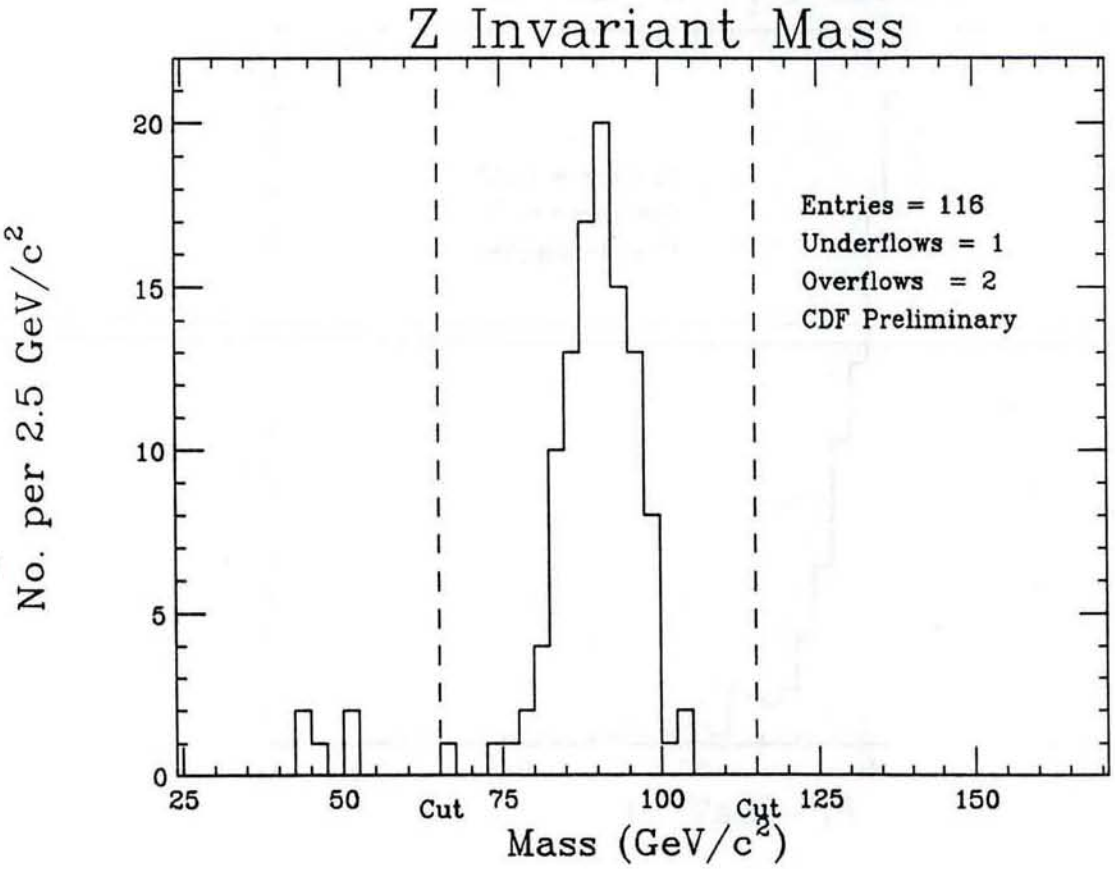

Figure 5: Dimuon invariant mass distribution for the $Z^\circ \rightarrow \mu^+\mu^-$ sample.

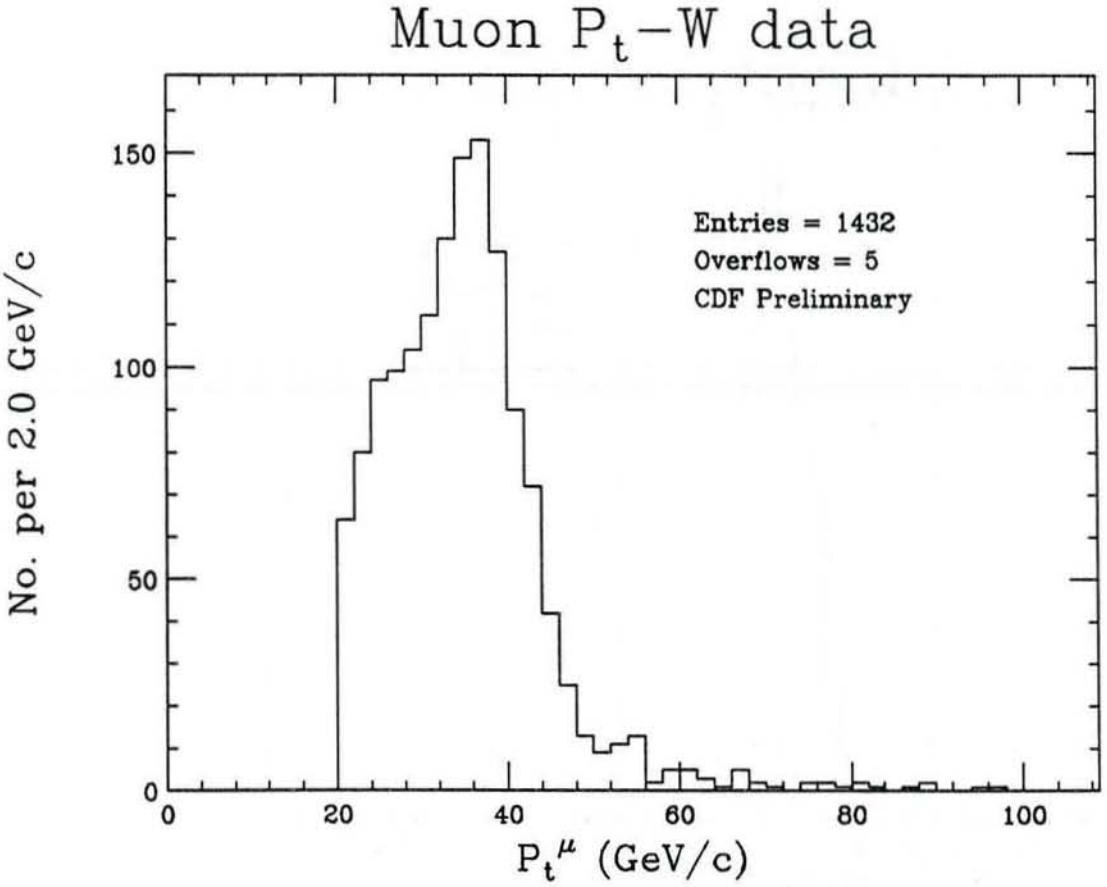

Figure 6: Muon transverse momentum distribution for the $W \rightarrow \mu\nu$ sample.

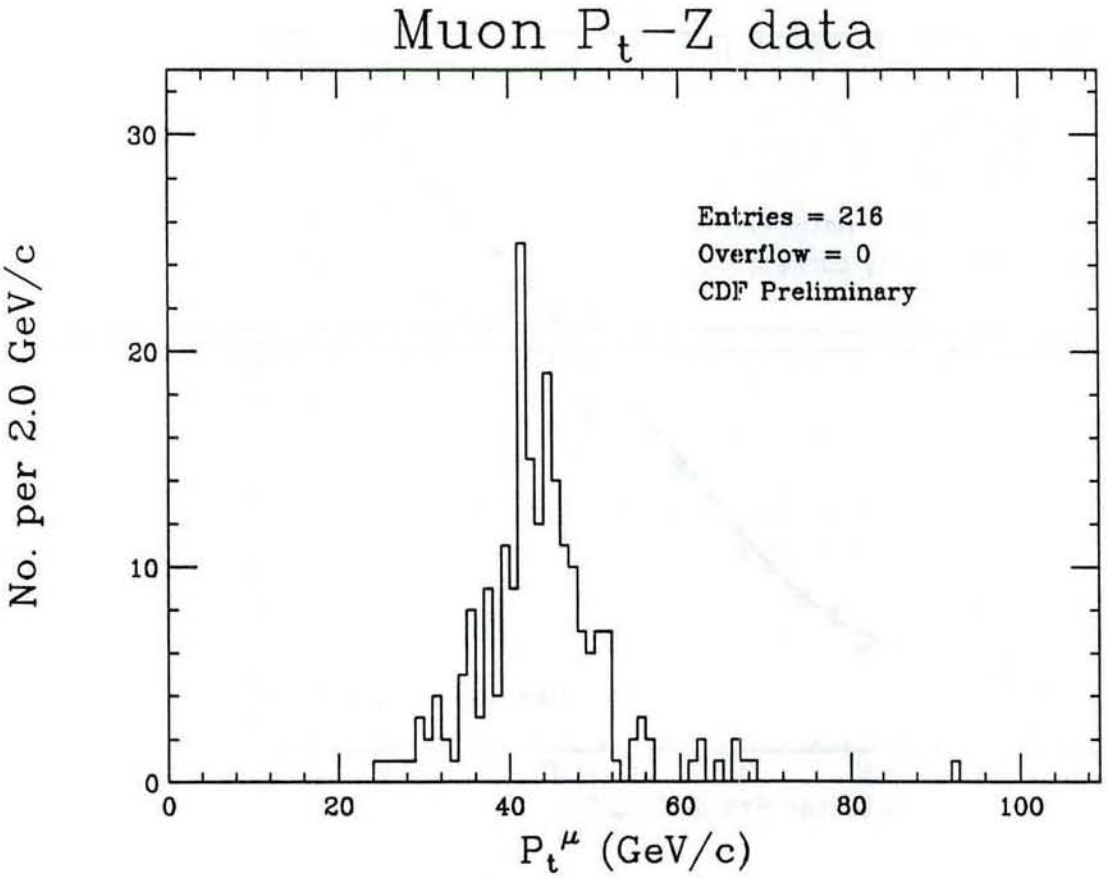

Figure 7: Muon transverse momentum distribution for the $Z^{\circ} \rightarrow \mu^{+}\mu^{-}$ sample.

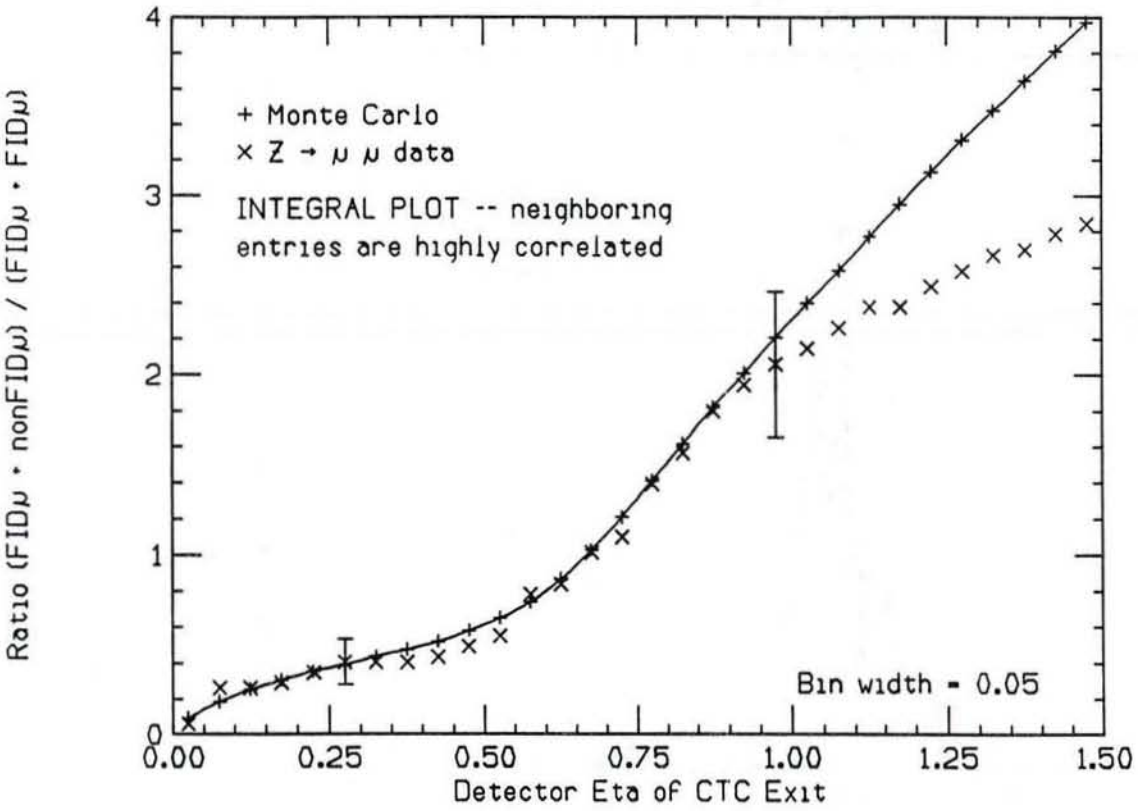

Figure 8: Ratio A_{0X}/A_{00} as a function of the high-η cut beyond which the second muon from the Z is not accepted.

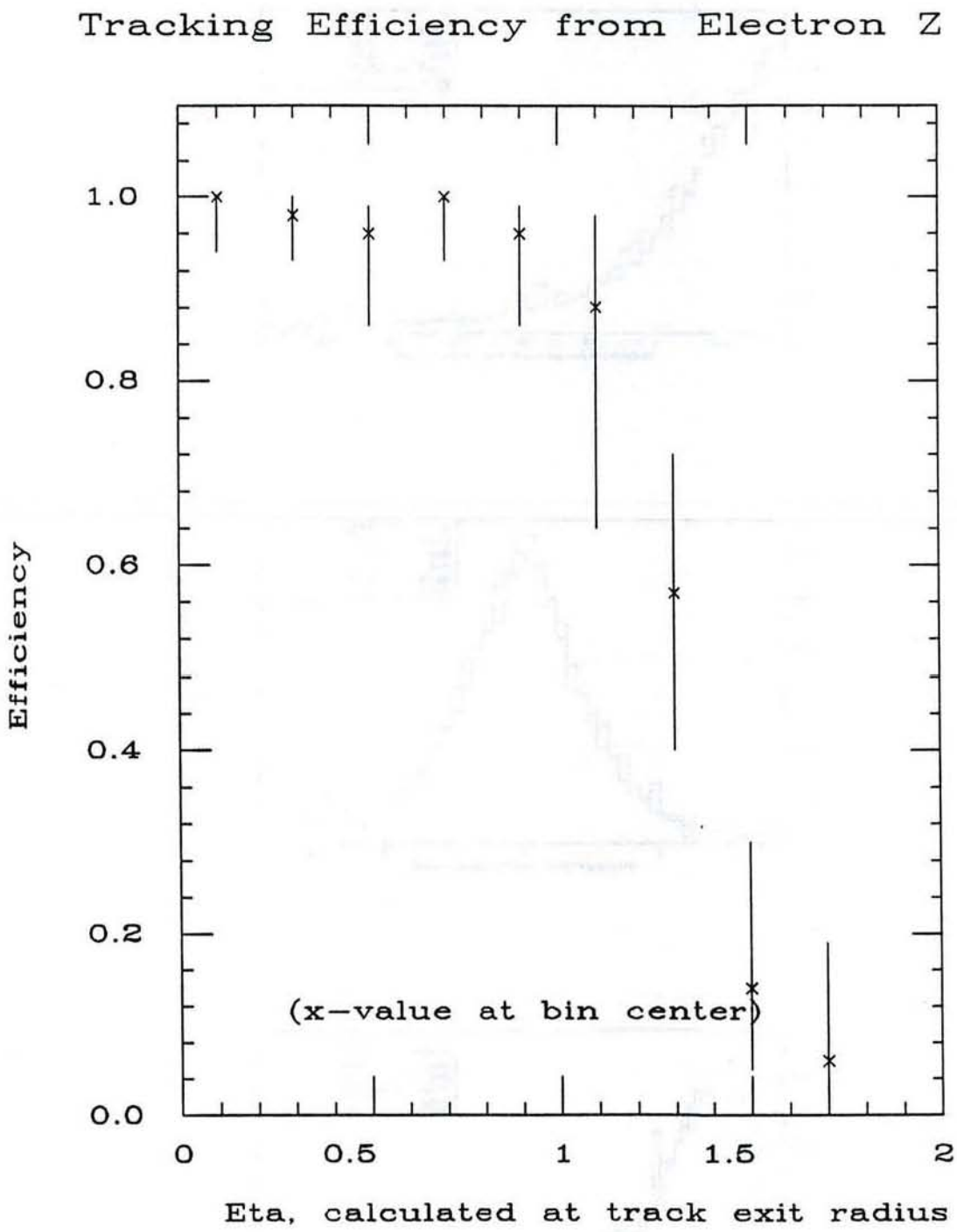

Figure 9: Tracking efficiency as a function of exit-radius η_e, using the second electron from $Z^\circ \rightarrow e^+e^-$ events.

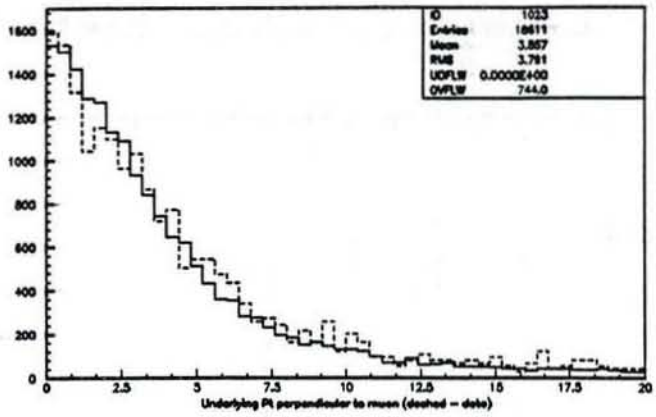

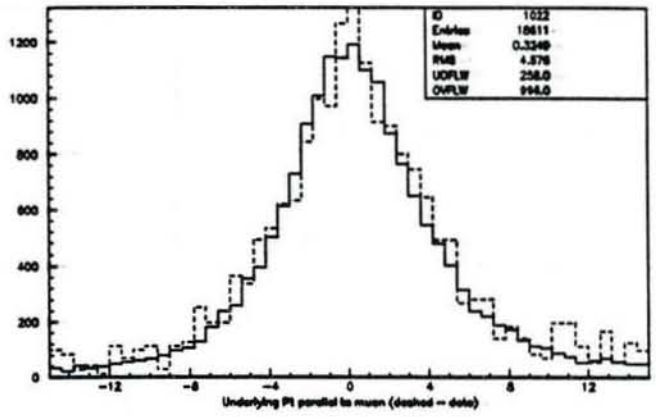

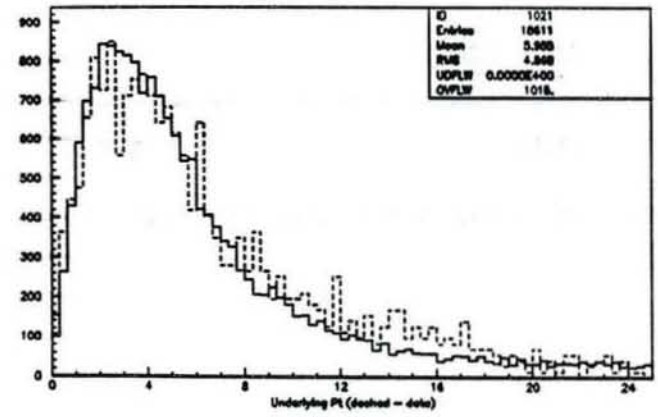

Figure 10: Comparison of underlying event energy for W sample (dash) and monte carlo (solid). Shown are the components perpendicular and parallel to the muon direction, as well as the scalar sum.

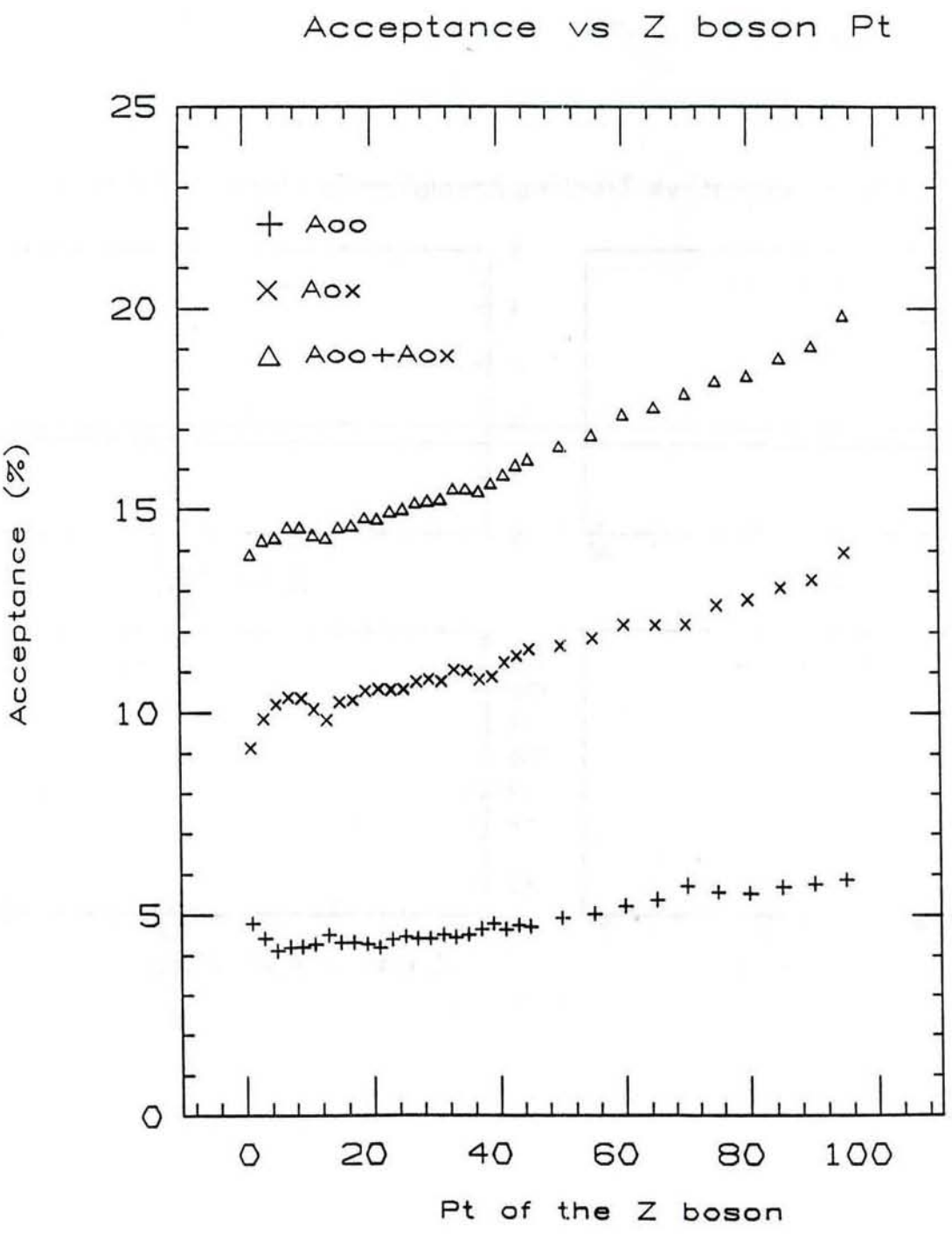

Figure 11: Z acceptance terms as a function of boson p_t. As boost increases opening angle shrinks and acceptance modulates over the 15° cracks.

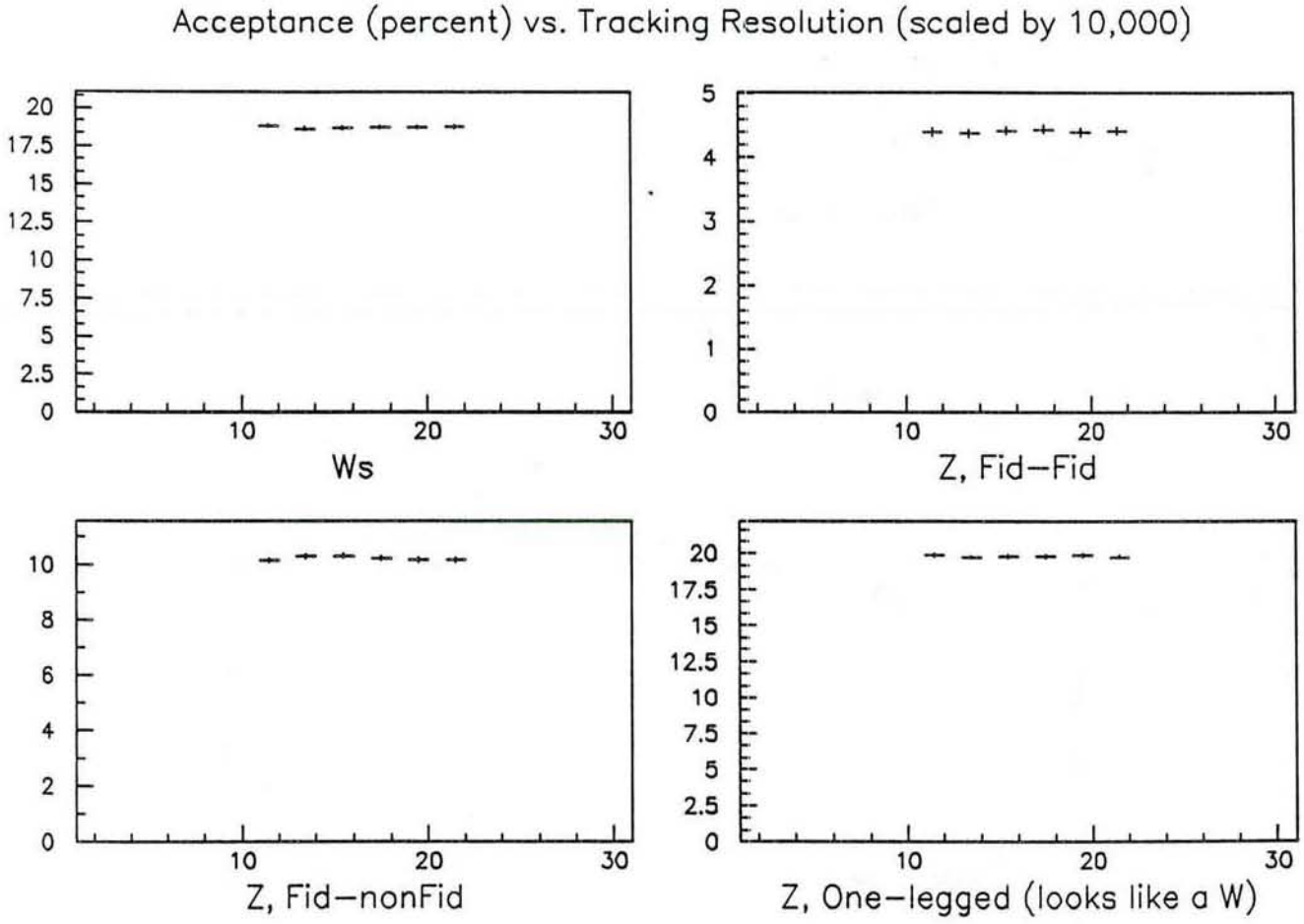

Figure 12: Acceptance versus tracking resolution.

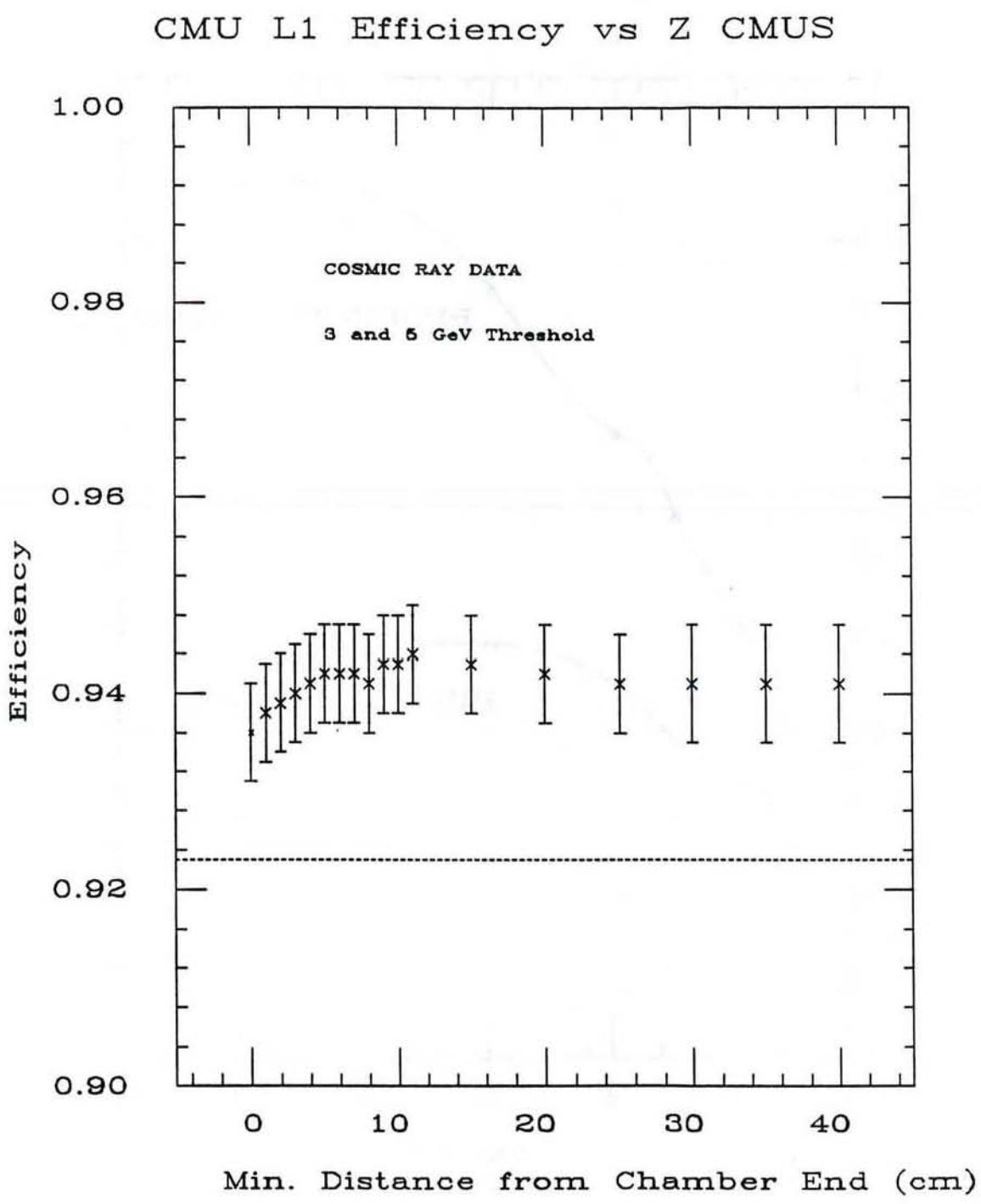

Figure 13: Level 1 trigger efficiency as a function of a cut away from the ends of the chambers, in z.

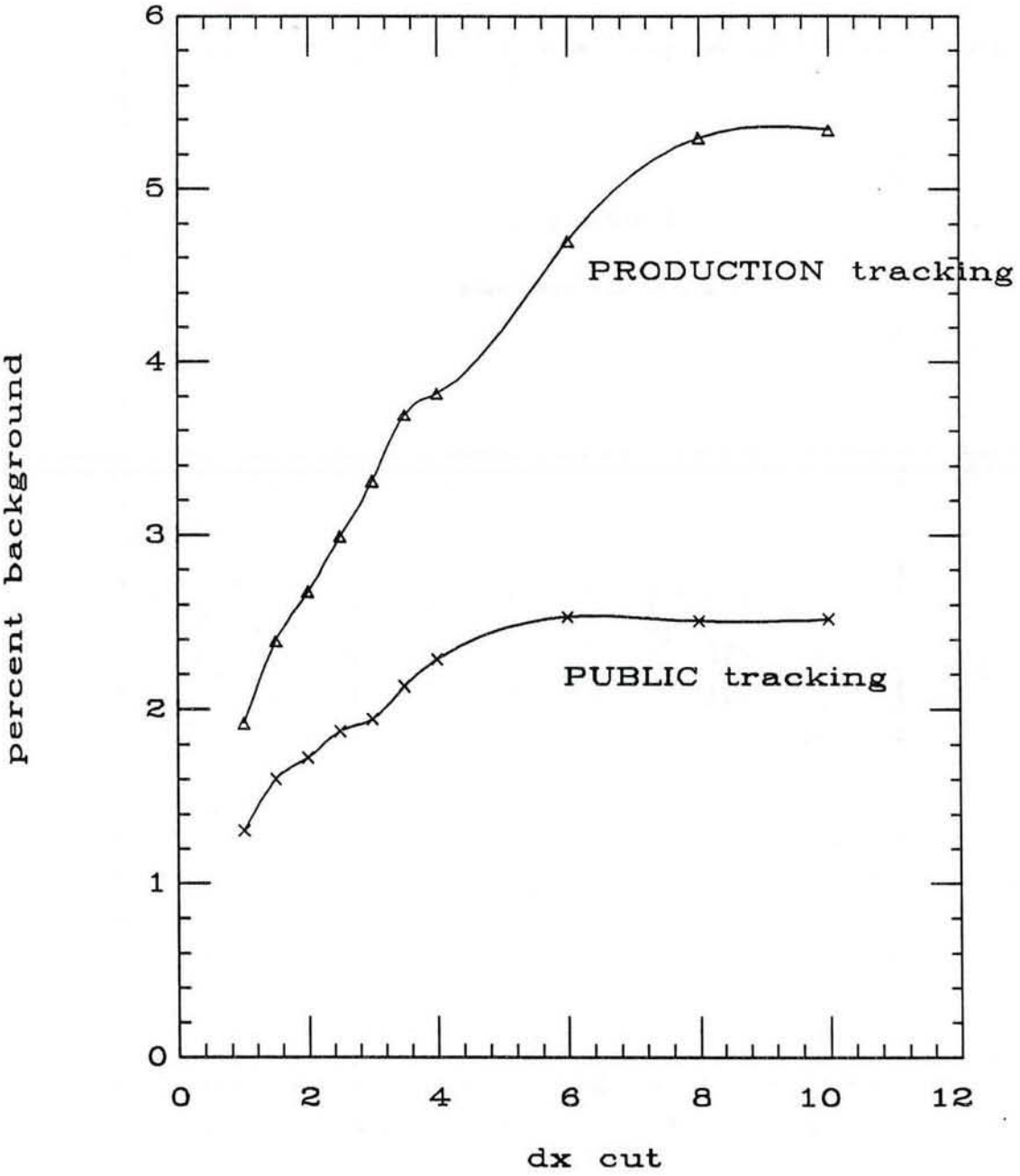

Figure 14: Estimate of W QCD background for different tracking, as a function of the CTC-CMU matching cut.

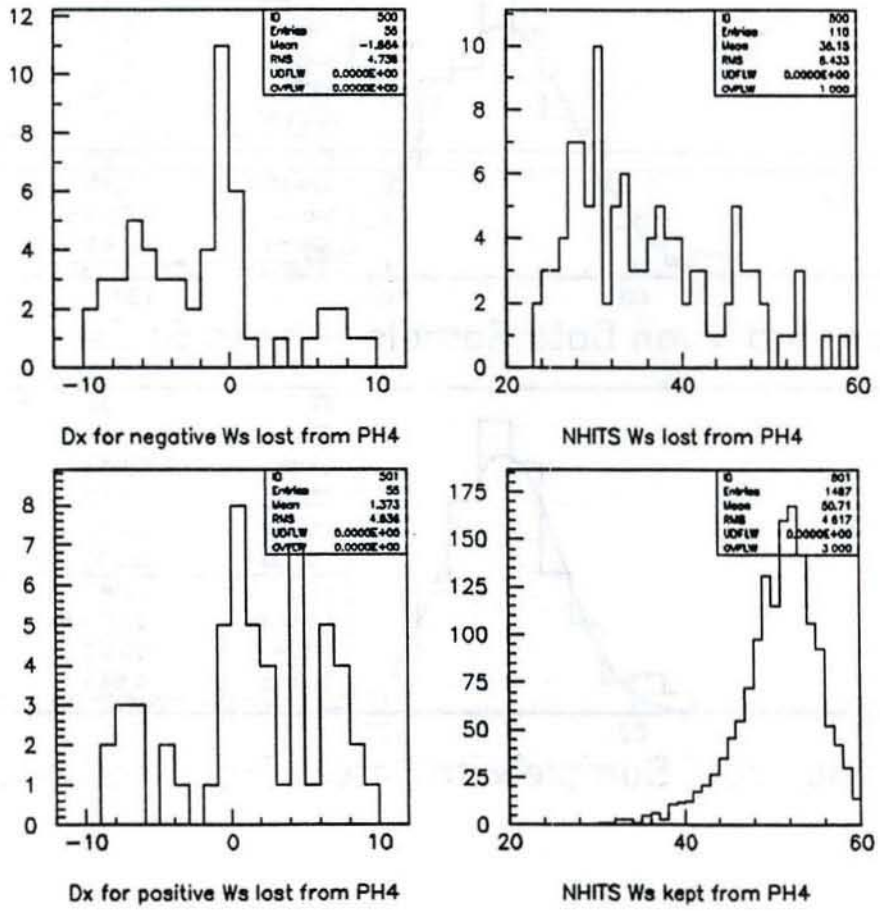

Figure 15: CMU-CTC track matching for μ^+ and μ^- candidates rejected by PUBLIC tracking, and comparison of CTC hit multiplicity for rejected and kept tracks.

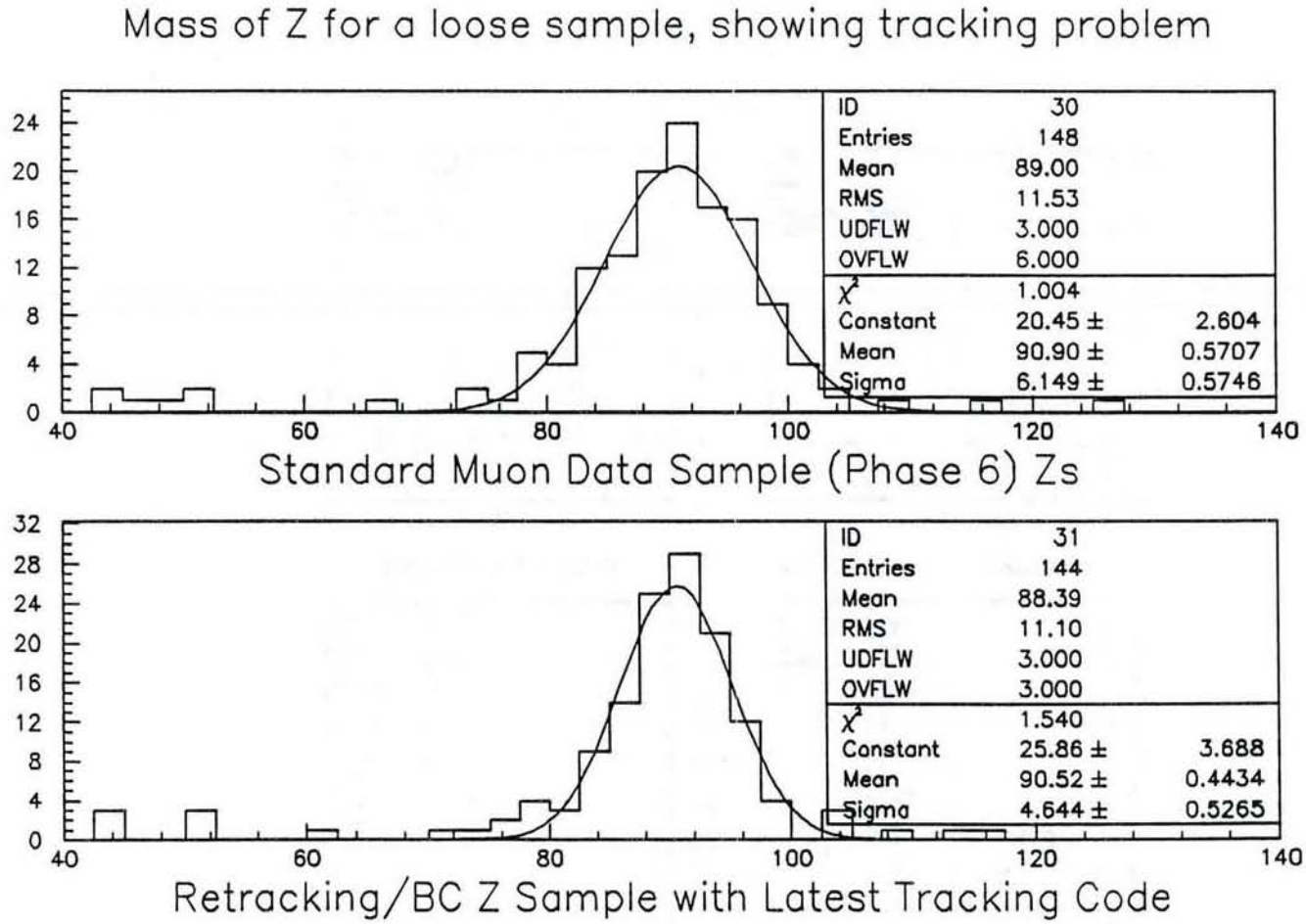

Figure 16: Dimuon mass distribution using PRODUCTION tracking and for our data sample (histograms). An error in the database code at the time of re-tracking gave the wrong beam position, degrading our observed resolution. Solid curve shows the resolution used in the acceptance monte carlo.

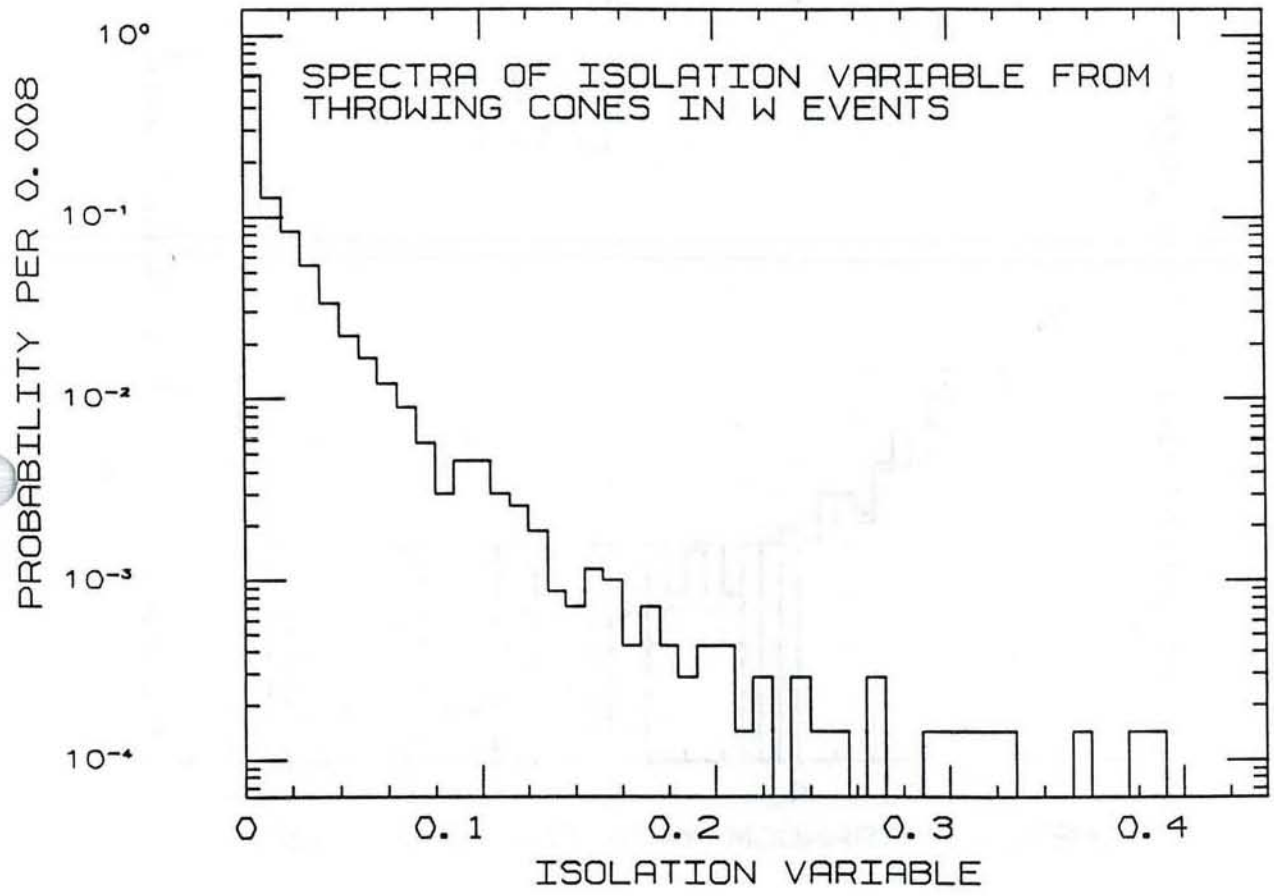

Figure 17: ISO spectrum from throwing cones.

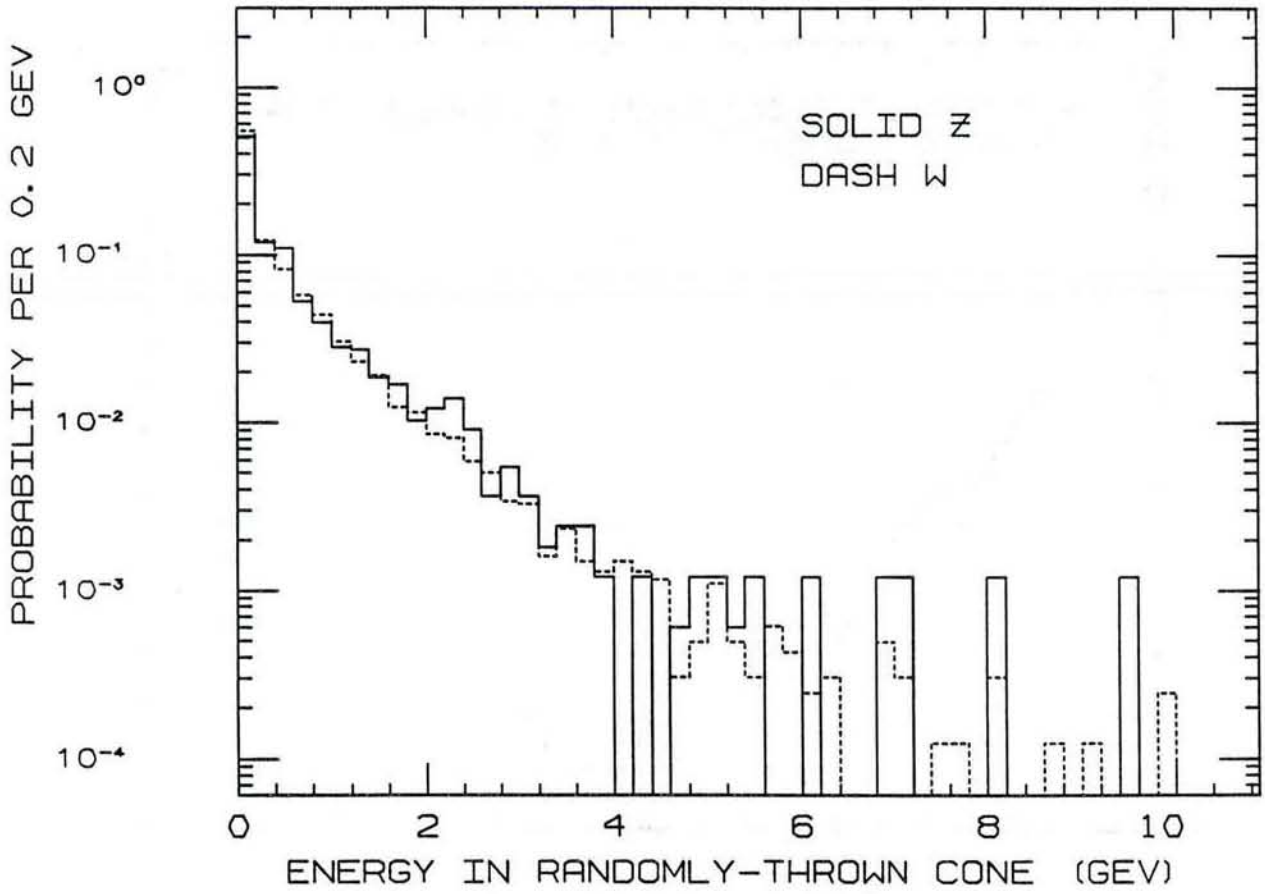

Figure 18: W and Z Econe spectra.

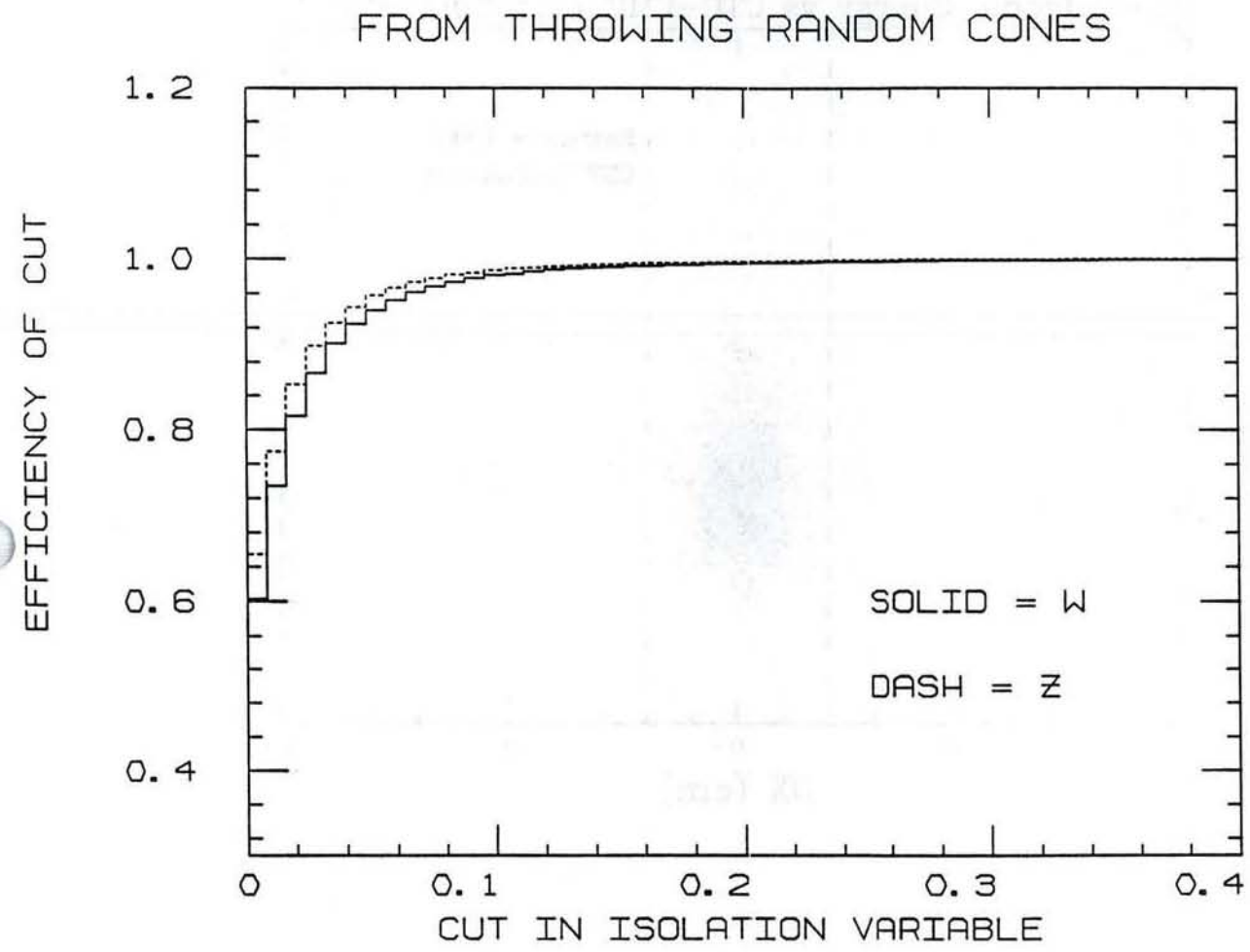

Figure 19: ε_{iso} versus ISO cut, using W Econe folded with $Z\, p_t^\mu$ (solid), and W Econe folded with $W\, p_t^\mu$ (dash).

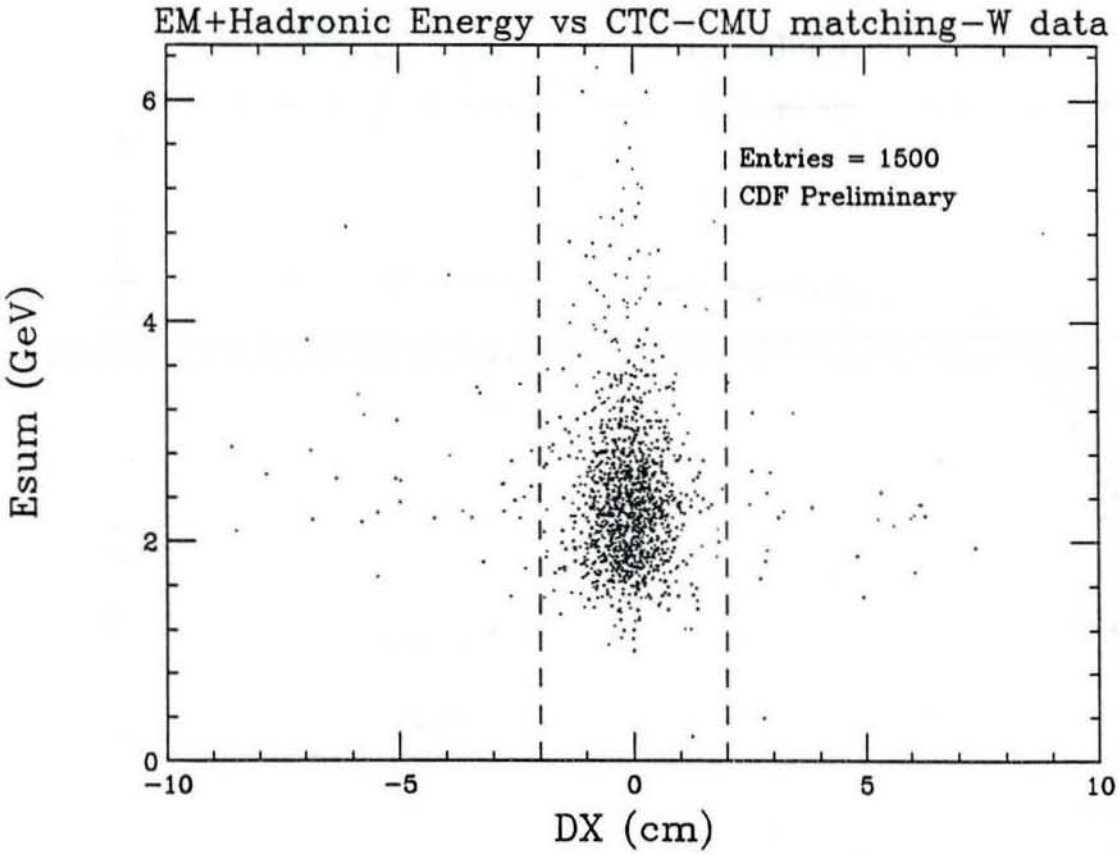

Figure 20: Energy deposition in the muon tower(EM+Had) vs CTC track/CMU stub match in the $r\phi$-plane for the W muons.

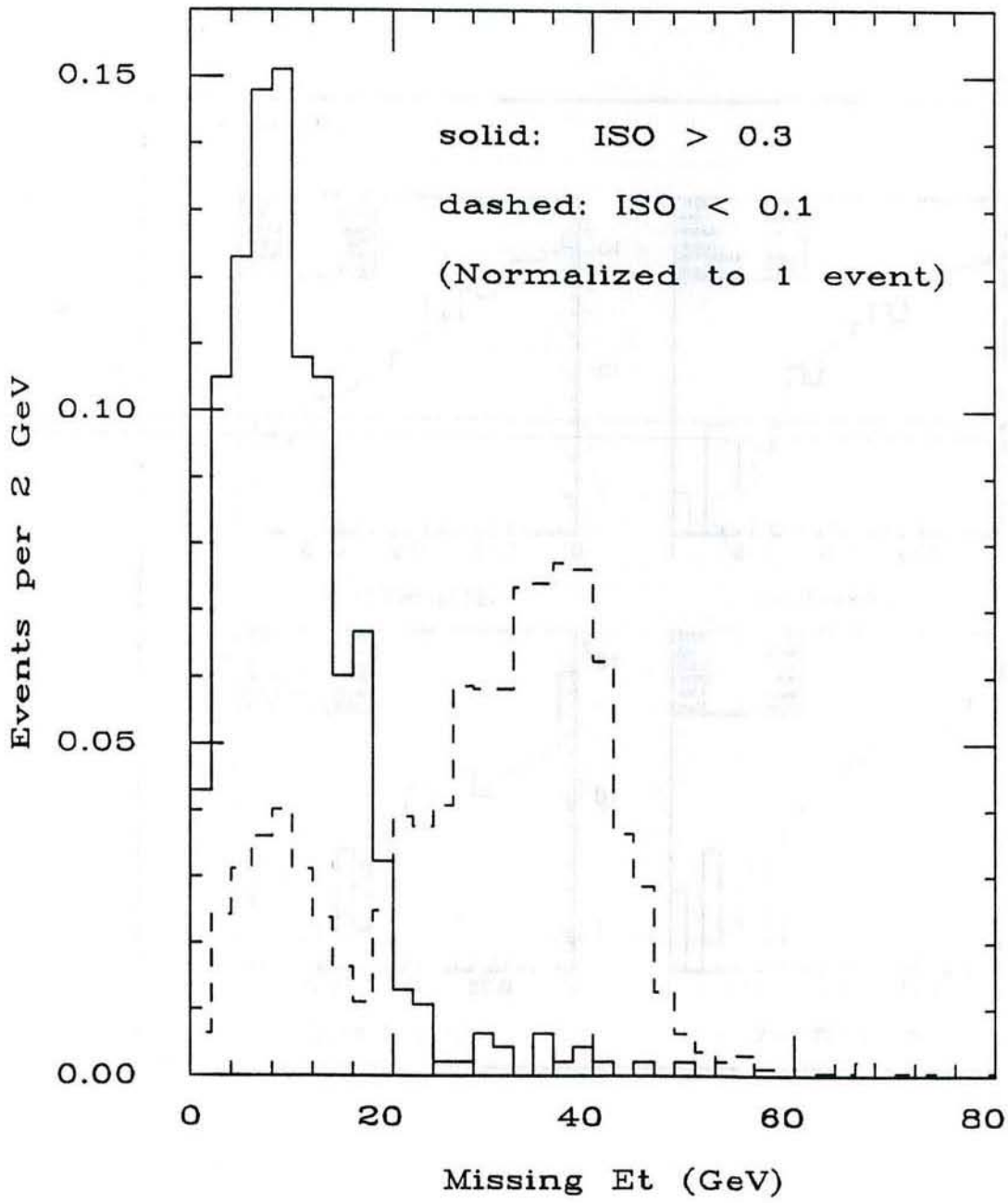

Figure 21: $dN/d\not{E}_T$ for isolated (solid) and non-isolated (dashed) muon candidates.

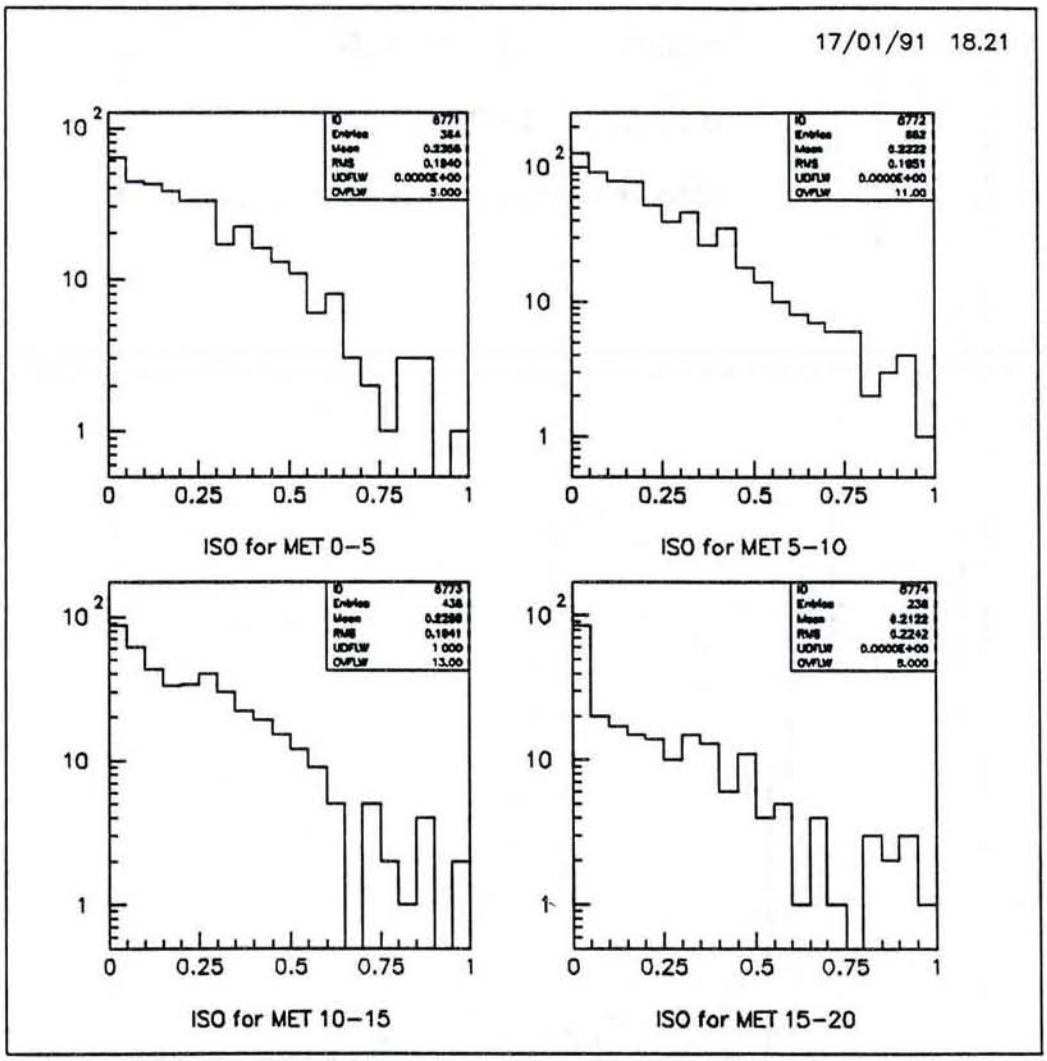

Figure 22: ISO distributions for 4 $\not\!\!E_T$ bins: a) $0 < \not\!\!E_T < 5$ GeV, b) $5 < \not\!\!E_T < 10$ GeV, c) $10 < \not\!\!E_T < 15$ GeV, d) $15 < \not\!\!E_T < 20$ GeV.

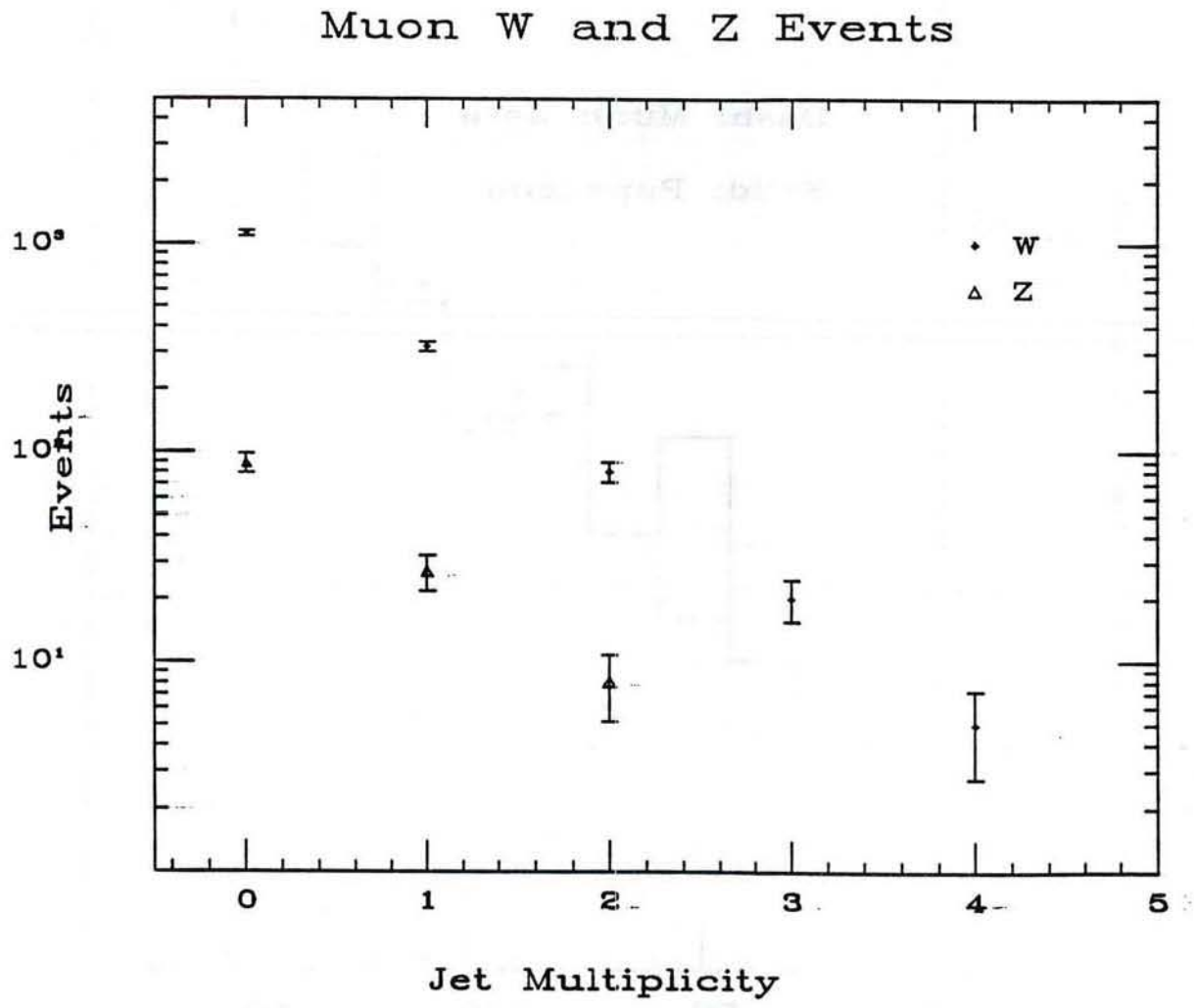

Figure 23: Jet multiplicity in W and Z events, requiring uncorrected jet $E_t > 10$ GeV.

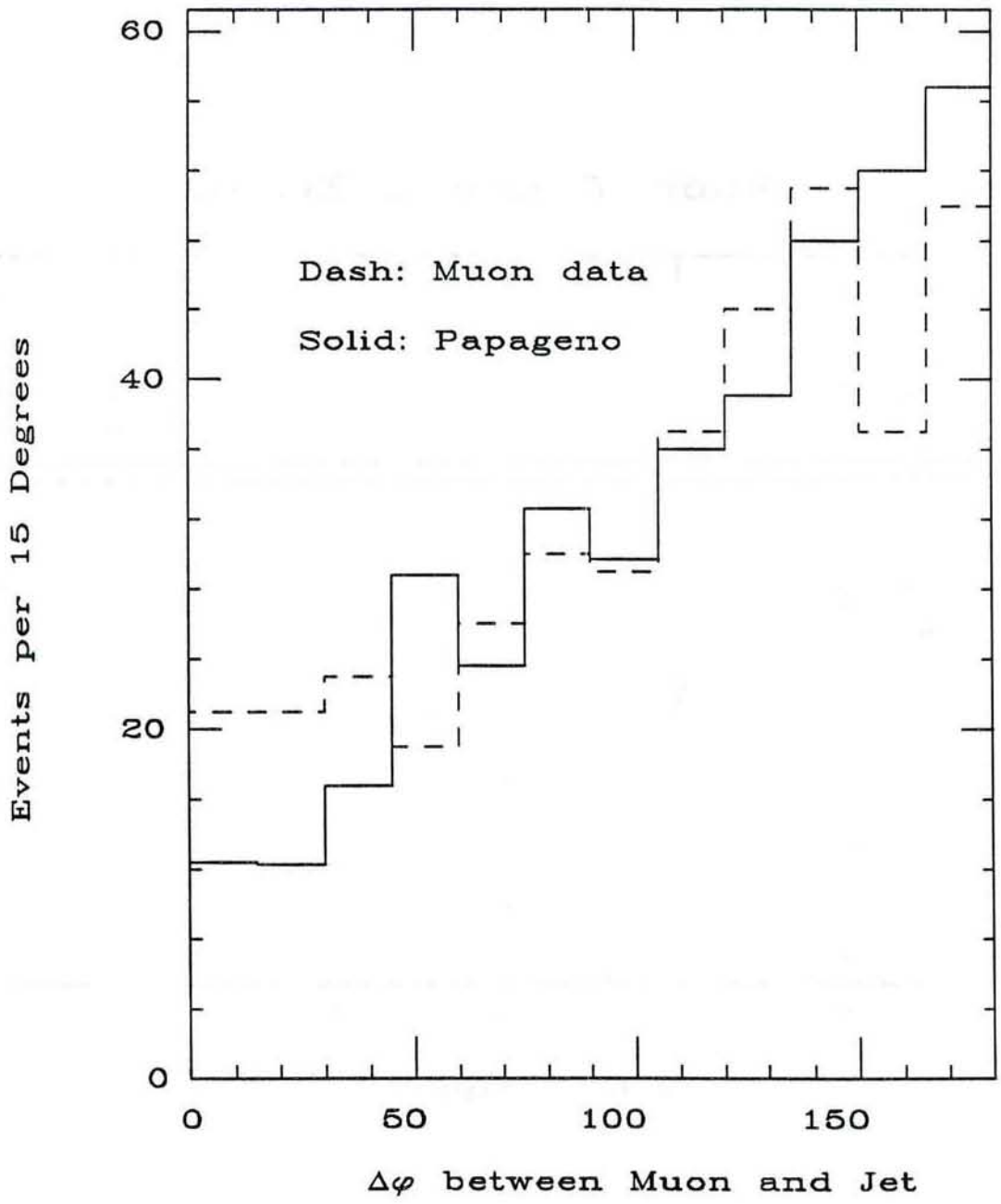

Figure 24: $\Delta\phi_{\mu j}$ for muon data overlayed with Papageno electrons, normalized to the number of muon events, muons are allowed near the leading jet.

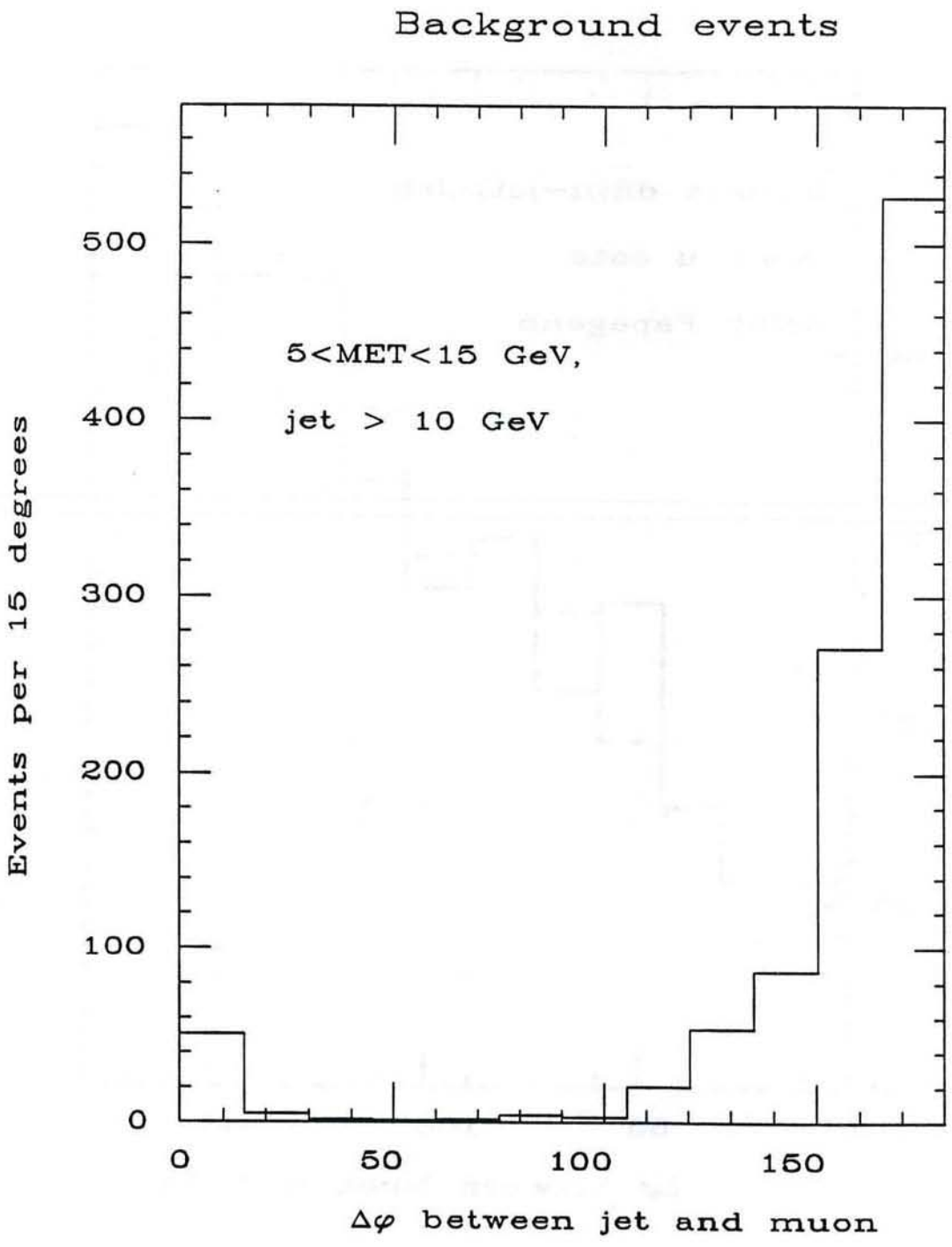

Figure 25: $\Delta\phi_{\mu j}$ for muon data outside the W region, $5 < \not\!\!E_{\rm T} < 15$ GeV.

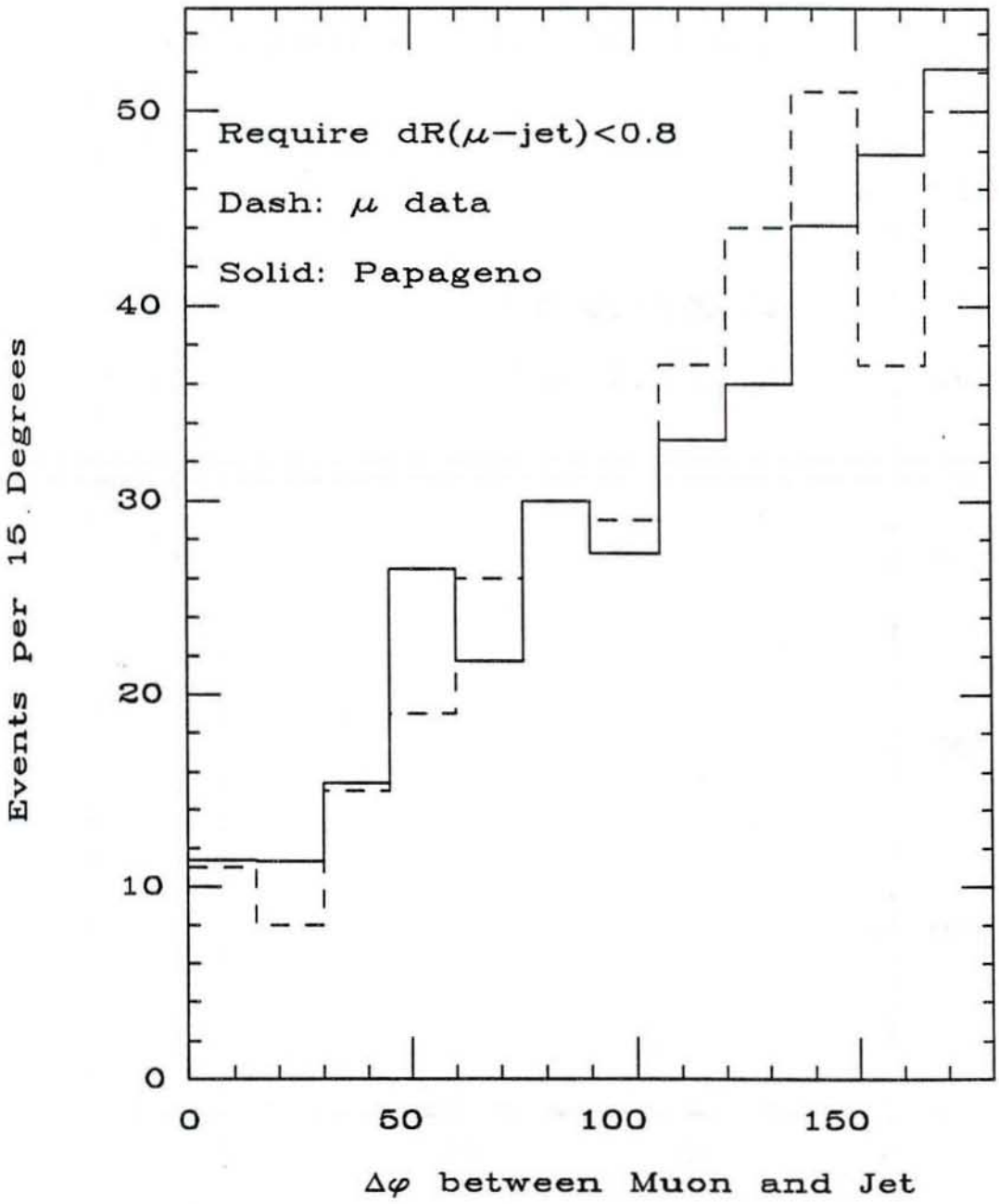

Figure 26: $\Delta\phi_{\mu j}$ for muon data overlayed with Papageno electron predictions. Muons near a jet are vetoed as for electrons. Monte Carlo normalized to number of muon events.

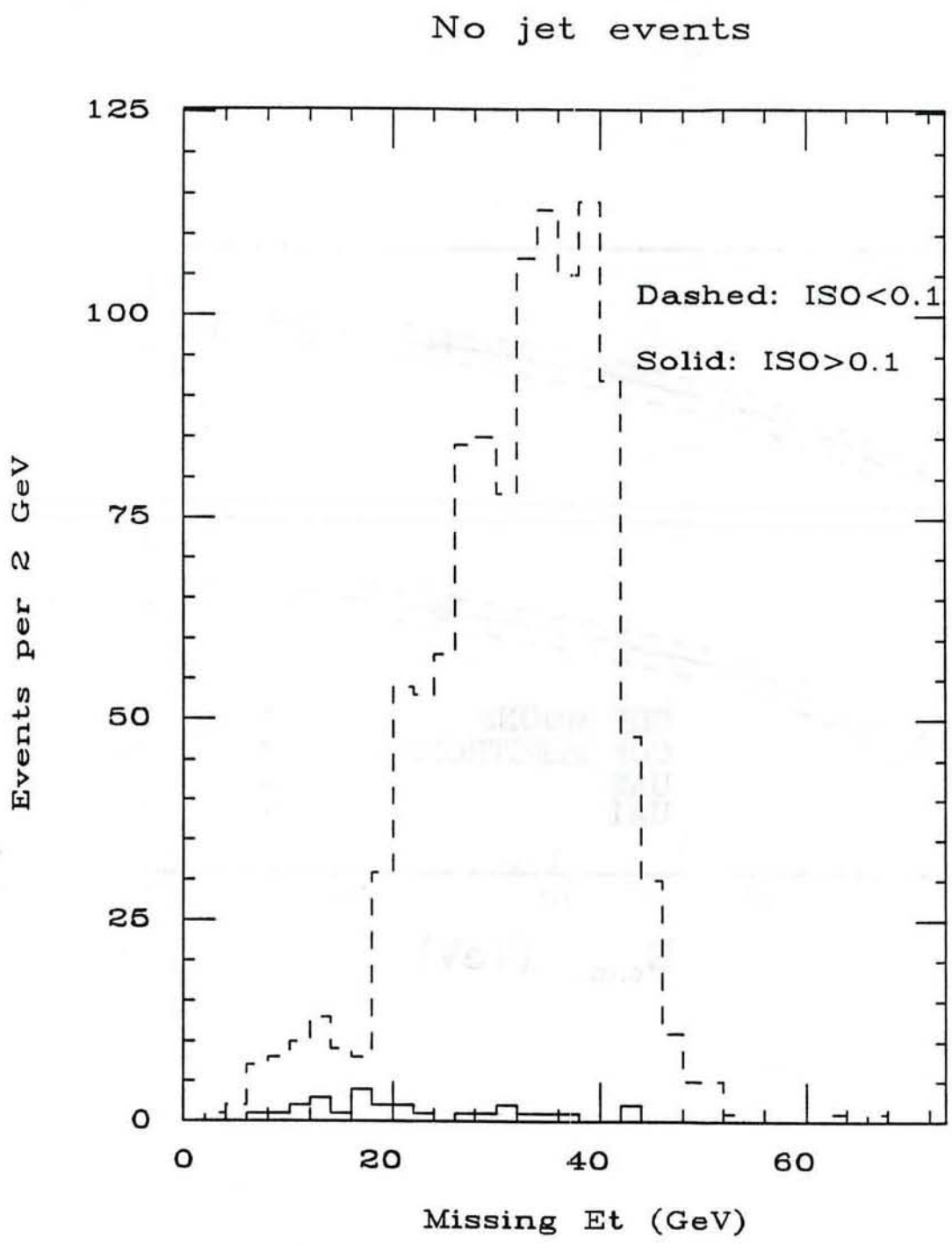

Figure 27: $\not\!\!E_T$ distribution for the no-jet sample. Solid is for $ISO < 0.1$, dashed is for $ISO > 0.1$

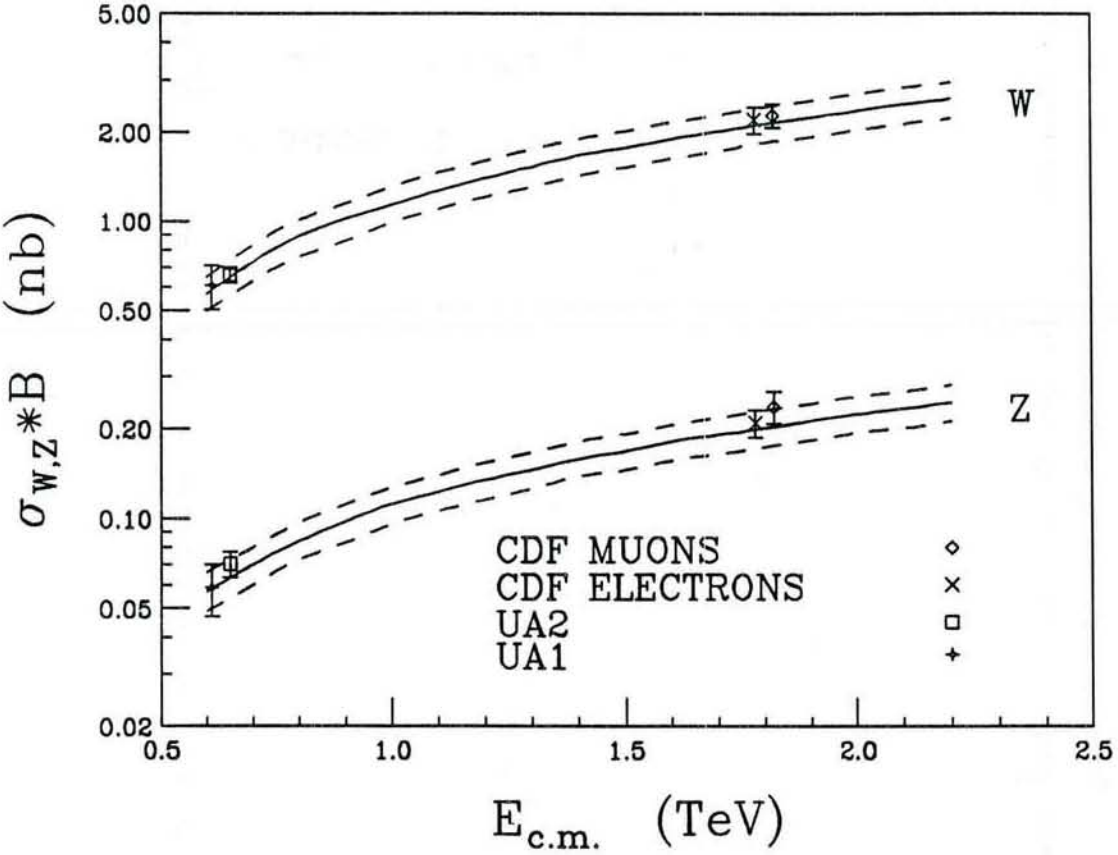

Figure 28: Partial cross-section versus c.m. energy. Curve is from Altarelli-Parisi, the dashed curves outline the 1σ band.

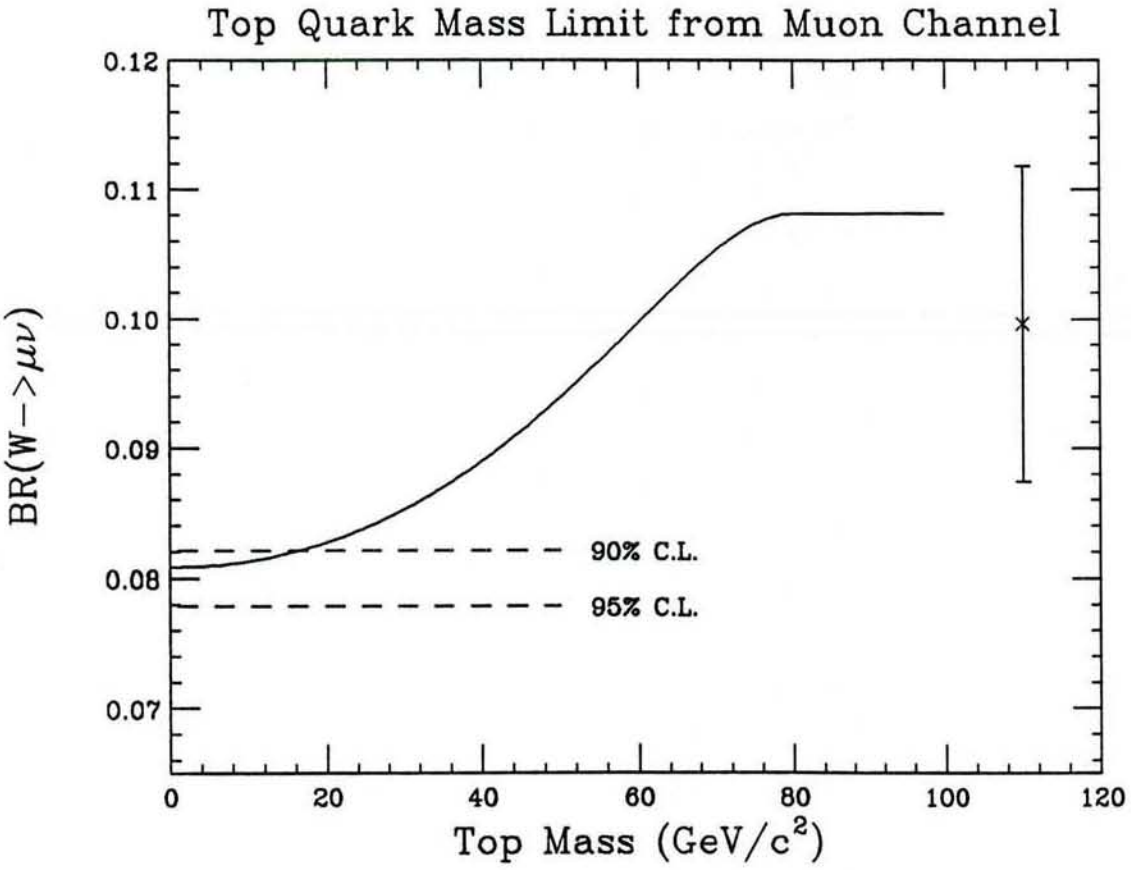

Figure 29: Theoretical prediction for W Branching Ratio to muons as a function of Top mass, along with the muon measurement.